Supplementary Information (SI) for Dalton Transactions.
This journal is © The Royal Society of Chemistry 2025

Synthesis, Spectral, and Electrochemical Studies of Electron-deficient Nitrile Porphyrins and the Utilization in Selective Cyanide Sensing

Varusha Bhardwaj, and Muniappan Sankar*

Department of Chemistry, Indian Institute of Technology Roorkee, Roorkee 247667, India.

Corresponding author's e-mail address: *m.sankar@cy.iitr.ac.in*

TABLE OF CONTENTS

Figure S14. The MALDI-TOF-MS of CuTPP(CN)(**1-Cu**) in positive ion mode at 298 K.

Figure S15. The MALDI-TOF-MS of ZnTPP(CN)(**1-Zn**) in positive ion mode at 298 K.

Figure S16. The MALDI-TOF-MS of H_2TPP(CN)$_2$(**2-H_2**) in positive ion mode at 298 K.

Figure S17. The MALDI-TOF-MS of CoTPP(CN)$_2$(**2-Co**) in positive ion mode at 298 K.

Figure S18. The MALDI-TOF-MS of NiTPP(CN)$_2$(**2-Ni**) in positive ion mode at 298 K.

Figure S19. The MALDI-TOF-MS of CuTPP(CN)$_2$(**2-Cu**) in positive ion mode at 298 K.

Figure S20. The MALDI-TOF-MS of ZnTPP(CN)$_2$(**2-Zn**) in positive ion mode at 298 K.

Figure S21. The HOMO-LUMO energies of the porphyrins calculated from electrochemical data.

Figure S22. The Crystal structure arrangement along (a) a-axis, (b) b-axis, and (c) c-axis. (Trapped solvent molecules are shown in between).

Figure S23. The H-bonding (inner N----H) Interaction in crystal packing.

Figure S24. Role of Hydrogen interactions in crystal packing arrangements as shown in different orientations.

Figure S25. Ground state optimized geometries of H_2TPP(CN)$_2$(**2-H_2**) and H_2TPP(CN)(**1-H_2**) using B3LYP as functional set and LANL2DZ as the basis set. Left side: top view and right side: side view.

Figure S26. Ground state optimized geometries of CoTPP(CN)$_2$(**2-Co**) and CoTPP(CN)(**1-Co**) using B3LYP as functional set and LANL2DZ as the basis set. Left side: top view and right side: side view.

Figure S27. Ground state optimized geometries of NiTPP(CN)$_2$(**2-Ni**) and NiTPP(CN)(**1-Ni**) using B3LYP as functional set and LANL2DZ as the basis set. Left side: top view and right side: side view.

Figure S28. Ground state optimized geometries of CuTPP(CN)$_2$(**2-Cu**) and CuTPP(CN)(**1-Cu**) using B3LYP as functional set and LANL2DZ as the basis set. Left side: top view and right side: side view.

Figure S29. Ground state optimized geometries of ZnTPP(CN)$_2$(**2-Zn**) and ZnTPP(CN)(**1-Zn**) using B3LYP as functional set and LANL2DZ as the basis set. Left side: top view and right side: side view.

Figure S30. Frontier molecular orbitals of H_2TPP(CN)(**1-H_2**).

Figure S31. Frontier molecular orbitals of CoTPP(CN)(**1-Co**).

Figure S32. Frontier molecular orbitals of NiTPP(CN)(**1-Ni**).

Figure S33. Frontier molecular orbitals of CuTPP(CN)(**1-Cu**).

Figure S34. Frontier molecular orbitals of ZnTPP(CN)(**1-Zn**).

Figure S35. Frontier molecular orbitals of $H_2TPP(CN)_2$(**2-H_2**).

Figure S36. Frontier molecular orbitals of $CoTPP(CN)_2$(**2-Co**).

Figure S37. Frontier molecular orbitals of $NiTPP(CN)_2$(**2-Ni**).

Figure S38. Frontier molecular orbitals of $CuTPP(CN)_2$(**2-Cu**).

Figure S39. Frontier molecular orbitals of $ZnTPP(CN)_2$(**2-Zn**).

Figure S40. The HOMO-LUMO energies of the porphyrins calculated form DFT calculation.

Figure S41. Calculated excitations (pink vertical lines) and experimental absorption spectra (black curve) for **1-H_2**.

Figure S42. Calculated excitations (pink vertical lines) and experimental absorption spectra (black curve) for **1-Co**.

Figure S43. Calculated excitations (pink vertical lines) and experimental absorption spectra (black curve) for **1-Ni**.

Figure S44. Calculated excitations (pink vertical lines) and experimental absorption spectra (black curve) for **1-Cu**.

Figure S45. Calculated excitations (pink vertical lines) and experimental absorption spectra (black curve) for **1-Zn**.

Figure S46. Calculated excitations (blue vertical lines) and experimental absorption spectra (black curve) for **2-H_2**.

Figure S47. Calculated excitations (blue vertical lines) and experimental absorption spectra (black curve) for **2-Co**.

Figure S48. Calculated excitations (blue vertical lines) and experimental absorption spectra (black curve) for **2-Ni**.

Figure S49. Calculated excitations (blue vertical lines) and experimental absorption spectra (black curve) for **2-Cu**.

Figure S50. Calculated excitations (blue vertical lines) and experimental absorption spectra (black curve) for **2-Zn**.

Figure S51. (a) Offset arrangement of molecules in crystal packing, and (b) Pie chart showing distribution of individual intermolecular interactions on the basis of hirshfeld surface analysis.

Figure S52. UV-vis spectra of parent porphyrins upon addition of excess cyanide in toluene at 298 K.

Figure S53. UV-vis spectra of porphyrins upon addition of excess cyanide and fluoride ions in toluene at 298 K.

Figure S54. Color change of the electron-deficient porphyrins, **1-Co** (1), **1-Zn** (2), **2-Co** (3) and **2-Zn** (4) in the presence of different anionic solutions in the toluene at 298 K and UV-visible spectral titrations upon addition of aliquots of TBACN (0-1× 10^{-5} M) in toluene (a), corresponding Hill plot (b) and B-H plot (c).

Figure S55. UV-visible spectra of **1-Co** (1), **1-Zn** (2), **2-Co** (3) and **2-Zn** (4) upon addition of cyanide ions and reversibility studies on addition of TFA.

Figure S56. MALDI-TOF negative ion mode mass spectrum of 2-Ni in presence of cyanide ions.

Figure S57. ^{1}H NMR titration of sensor **2-Ni** (5 mM) in $CDCl_3$ with adding 0 to 2.5 equivalence of TBACN.

Figure S58. Photographs of test kits with **2-Ni** (1 mM) for detecting the cyanide ion in (a) toluene solution (above) and (b) neutral aqueous solution (below) with other anions.

Figure S59. Frontier molecular orbitals of **2-Ni•2CN^{-}**

Table S1. Data of selected bond angles (º) and bond lengths (Å) calculated from the single crystal XRD data analysis.

Table S2. Data of selected bond angles (º) and bond lengths (Å) calculated from ground state optimized geometries using B3LYP as functional and LANL2DZ as basis set.

Table S3. TD-DFT calculated one-electron transitions and oscillator strengths of monocyano porphyrin and dicyanoporphyrins. (f > 0.01).

Synthetic Procedures

Synthesis of (7-cyano-5,10,15,20-tetraphenylporphyrin)copper(II) (1-Cu) and (7,8-dicyano-5,10,15,20-tetraphenylporphyrin)copper(II) (2-Cu): To a 250 ml round bottom flask, 500 mg of H_2TPP was dissolved in 25 ml of chloroform and subsequently NBS(1.5 equiv.) dissolved in chloroform was dropwise added to the reaction mixture while refluxing. The reaction was monitored using TLC and absorption features. It gave an inseparable mixture of mono and dibromo substituted porphyrin (1-Br, and 2-Br) in good yields. The mixture was purified using flash chromatography. Further, it was applied for direct cyanation using cuprous cyanide (25 equiv.) in quinoline as solvent medium. After 4 hrs., the reaction was completed as indicated by the TLC. The reaction mixture was quenched by 2M HCl and aqueous work up was performed to extract the desired product in the organic layer. The mixture of 1-Cu and 2-Cu thus obtained was purified by the silica gel chromatography using 1:1 chloroform:hexane solvent as the eluent.

(1-Cu): Yield: 0.200 g (35 %). UV-Vis. (λ_{max} in nm): 422 (5.52), 548 (4.41), 585 (4.24). MALDI-TOF-MS: *m/z* 701.53 for $[M+H]^+$ (calculated 701.16).

(2-Cu): Yield: 0.106 g (18 %). UV-Vis. (λ_{max} in nm): 435 (5.22), 561 (3.82), 607 (4.22). MALDI-TOF-MS: *m/z* 725.29 for $[M+H]^+$ (calculated 725.12).

Synthesis of 5,10,15,20-tetraphenylporphyrin-7-carbonitrile (1-H_2): In a 100 ml round bottom flask, 180 mg of 1-Cu was taken and stirred in chloroform on ice-bath. Dropwise addition of Conc.H_2SO_4 to the reaction mixture yielded demetallated product in excellent yield. The product was purified on silica gel column chromatography using chloroform as the eluent. Yield: 0.150 g (91 %). UV-Vis. (λ_{max} in nm): 424 (5.04), 523 (4.26), 559 (2.61), 602 (3.70), 658 (4.02). ^{1}H NMR (500 MHz, $CDCl_3$) δ 9.37 (s, 1H, β-pyrrolic proton), 8.98 (d, *J* = 4.8 Hz, 1H, β-pyrrolic proton), 8.95 – 8.90 (m, 3H, β-pyrrolic proton), 8.74 (s, 2H, β-pyrrolic proton), 8.18 (d, *J* = 7.1 Hz, 8H, , *o*-Ph protons), 7.93 (d, *J* = 7.1 Hz, 1H, , *m*-Ph proton), 7.91 – 7.61 (m, 11H, *m*- and *p*-Ph protons), -2.72 (s, 2H, NH protons). MALDI-TOF-MS: *m/z* 640.39 for $[M+H]^+$ (calculated 640.24).

Synthesis of (7-cyano-5,10,15,20-tetraphenylporphyrin)cobalt(II) (1-Co) : 20 mg of 1-H_2 was dissolved in 5 ml. of chloroform and 10 equiv. of cobalt acetate (62 mg) was taken in methanol. The reaction medium was refluxed on water bath for 30 min. The metalation was confirmed by the change in the number of Q bands. After the aqueous work up, the product was purified using column chromatography with chloroform as the eluting medium. Yield: 0.014 g (65 %). UV-Vis. (λ_{max} in nm): 418(5.49), 537 (4.31), 571 (4.13). MALDI-TOF-MS: *m/z* 697.26 for $[M+H]^+$ (calculated 697.16).

Synthesis of (7-cyano-5,10,15,20-tetraphenylporphyrin)nickel(II) (1-Ni): 20 mg of 1-H_2 and 10 equiv. of nickel acetate (77 mg) was taken in DMF as the solvent. The reaction mixture was refluxed for 4 hrs. After cooling the reaction medium, distilled water was added to the mixture. The precipitate thus obtained was filtered through the crucible and was purified using column chromatography with chloroform as the eluting medium. Yield: 0.016 g (74 %). UV-Vis. (λ_{max} in

nm): 422 (5.44), 537 (4. 31), 572 (4.12). ^{1}H NMR (500 MHz, $CDCl_3$) δ 9.26 (s, 1H), 8.83 (d, *J* = 5.0 Hz, 1H), 8.75 – 8.65 (m, 5H), 8.00 – 7.92 (m, 8H), 7.83 (t, *J* = 7.6 Hz, 1H), 7.70 (td, *J* = 13.2, 6.5 Hz, 11H). MALDI-TOF-MS: *m/z* 696.31 for $[M+H]^+$ (calculated 696.16).

Synthesis of (7-cyano-5,10,15,20-tetraphenylporphyrin)zinc(II) (1-Zn): 20 mg of 1-H_2 was dissolved in 5 ml. of chloroform and 10 equiv. of zinc acetate (78 mg) was taken in methanol. The reaction medium was refluxed on water bath for 15 min. The metalation was confirmed by the change in the number of Q bands. After the aqueous work up, the product was purified using column chromatography with chloroform as the eluting medium. Yield: 0.017 g (78 %). UV-Vis. (λ_{max} in nm): 425 (5.58), 557 (4.56), 595 (4.37). ^{1}H NMR (500 MHz, $CDCl_3$) δ 9.44 (s, 1H), 8.96 – 8.85 (m, 6H), 8.20 – 8.09 (m, 8H), 7.79 (m, 12H). MALDI-TOF-MS: *m/z* 702.60 for $[M+H]^+$ (calculated 702.16).

Synthesis of 5,10,15,20-tetraphenylporphyrin-7,8-dicarbonitrile (2-H_2): In a 100 ml round bottom flask, 90 mg of 2-Cu was taken and stirred in chloroform on ice-bath. Dropwise addition of conc. H_2SO_4 to the reaction mixture yielded demetallated product in excellent yield. The product was purified on silica gel column chromatography using chloroform as the eluent. Yield: 0.078 g (95 %). UV-Vis. (λ_{max} in nm): 441 (4.51), 537 (3.16), 578 (2.76), 633 (2.64), 691 (3.21). ^{1}H NMR (500 MHz, $CDCl_3$) δ 8.97 (d, *J* = 5.1 Hz, 2H), 8.89 (d, *J* = 5.1 Hz, 2H), 8.69 (s, 1H), 8.18 (ddd, *J* = 6.3, 3.8, 1.3 Hz, 8H), 7.97 (t, *J* = 7.7 Hz, 2H), 7.85 – 7.78 (m, 10H). MALDI-TOF-MS: *m/z* 664.37 for $[M+H]^+$ (calculated 664.24).

Synthesis of (7,8-dicyano-5,10,15,20-tetraphenylporphyrin)cobalt(II) (2-Co): 15 mg of 2-H_2 was dissolved in 5 ml. of chloroform and 10 equiv. of cobalt acetate (56 mg) was taken in methanol. The reaction medium was refluxed on water bath for 30 min. The product was purified using column chromatography with chloroform as the eluting medium. Yield: 0.012 g (74 %). UV-Vis. (λ_{max} in nm): 431 (5.64), 554 (4.36), 596 (4.69). MALDI-TOF-MS: *m/z* 721.28 for $[M+H]^+$ (calculated 721.16).

Synthesis of (7,8-dicyano-5,10,15,20-tetraphenylporphyrin)nickel(II) (2-Ni): 20 mg of 2-H_2 and 10 equiv. of nickel acetate (75 mg) was taken in DMF as the solvent. The reaction mixture was refluxed for 4 hrs. After cooling the reaction medium, distilled water was added to the mixture. The precipitate thus obtained was filtered through the crucible and was purified using column chromatography with chloroform as the eluting medium. Yield: 0.014 g (65 %). UV-Vis. (λ_{max} in nm): 434 (5.34), 519 (3.78), 555 (4.04), 598 (4.44). ^{1}H NMR (500 MHz, $CDCl_3$) δ 8.74 (d, *J* = 5.1 Hz, 2H), 8.65 (s, 2H), 8.58 (d, *J* = 5.1 Hz, 2H), 7.94 – 7.87 (m, 8H), 7.82 (t, *J* = 7.6 Hz, 2H), 7.74 – 7.65 (m, 10H). MALDI-TOF-MS: *m/z* 720.29 for $[M+H]^+$ (calculated 720.16).

Synthesis of (7,8-dicyano-5,10,15,20-tetraphenylporphyrin)zinc(II) (2-Zn): 20 mg of 2-H_2 was dissolved in 5 ml. of chloroform and 10 equiv. of zinc acetate (66 mg) was taken in methanol. The reaction medium was refluxed on water bath for 20 min. The product was purified using column chromatography with chloroform as the eluting medium.Yield: 0.018 g (82 %). UV-Vis. (λ_{max} in

nm): 441 (5.47), 571 (3.94), 617 (4.29). ^{1}H NMR (500 MHz, $CDCl_3$) δ 8.83 – 8.73 (m, 6H), 8.10 (dd, *J* = 22.6, 6.7 Hz, 8H), 7.89 (t, *J* = 7.6 Hz, 2H), 7.80 – 7.72 (m, 10H). MALDI-TOF-MS: *m/z* 726.27 for $[M+H]^+$ (calculated 726.15).

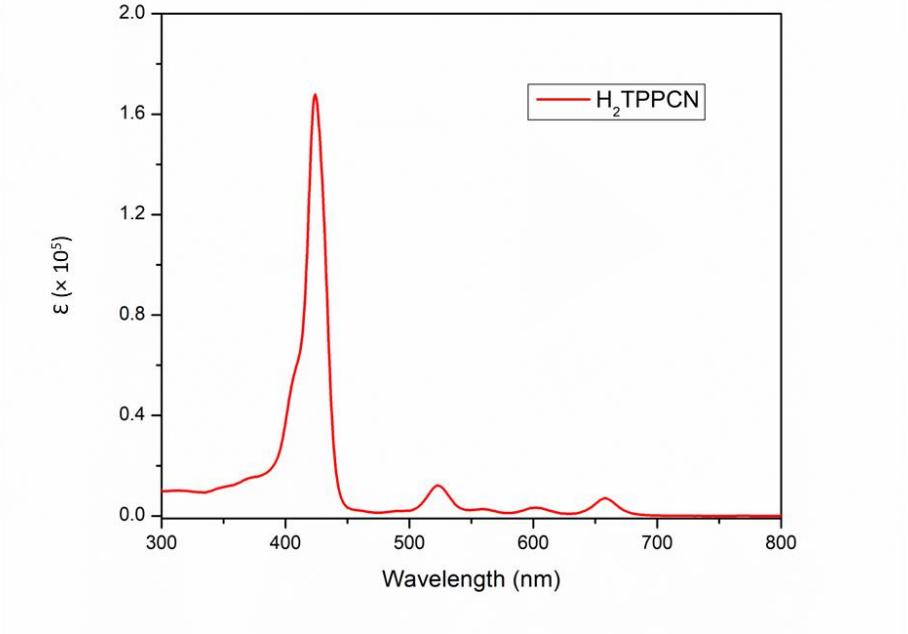

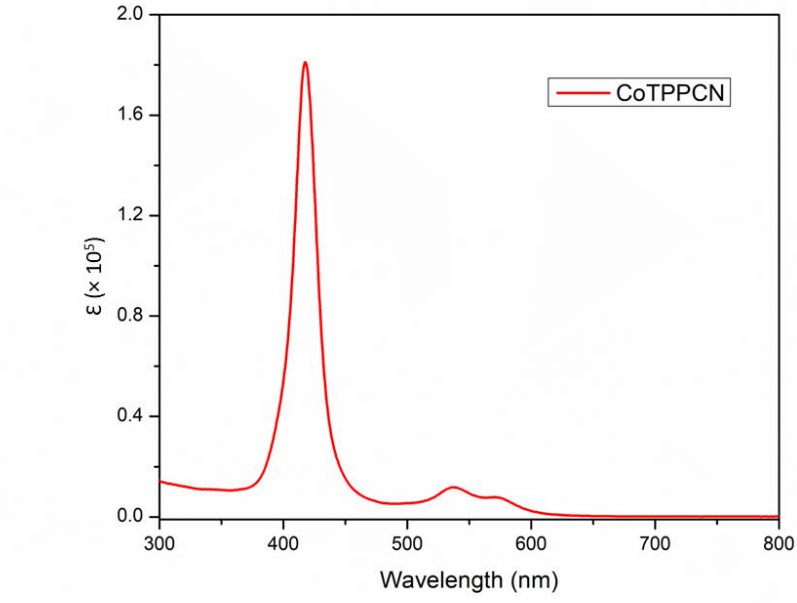

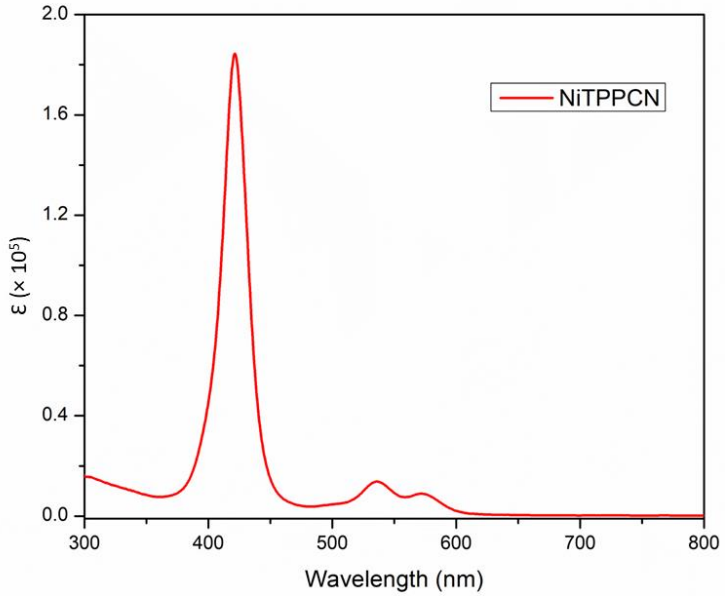
NiTPPCN
ε (× 10⁵)
Wavelength (nm)
2.0
1.6
1.2
0.8
0.4
0.0
300
400
500
600
700
800

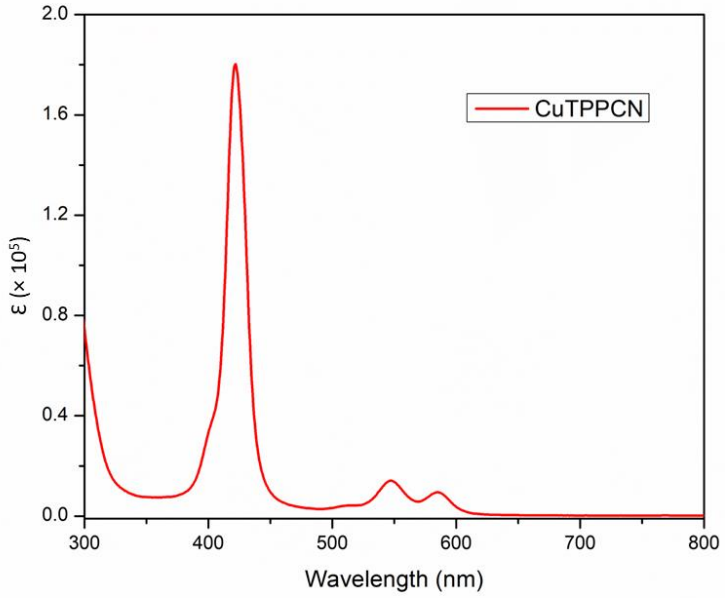
CuTPPCN
ε (× 10⁵)
Wavelength (nm)
2.0
1.6
1.2
0.8
0.4
0.0
300
400
500
600
700
800

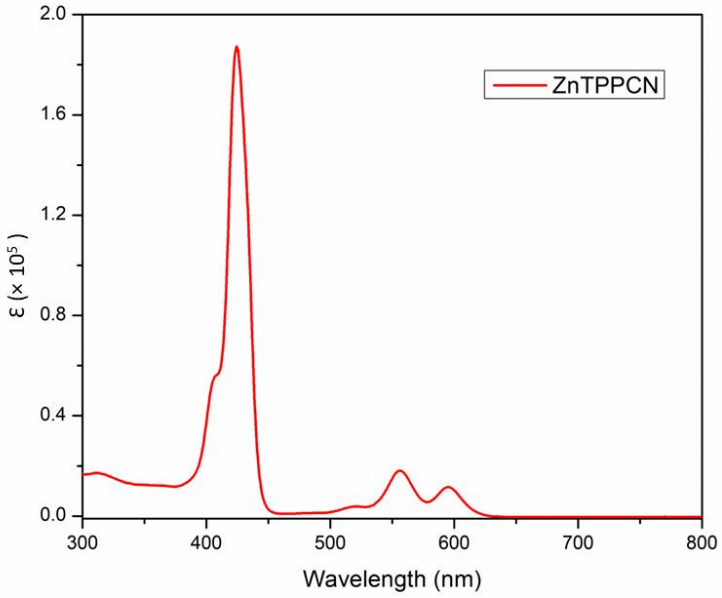
ZnTPPCN
ε (× 10^5)
Wavelength (nm)
2.0
1.6
1.2
0.8
0.4
0.0
300
400
500
600
700
800

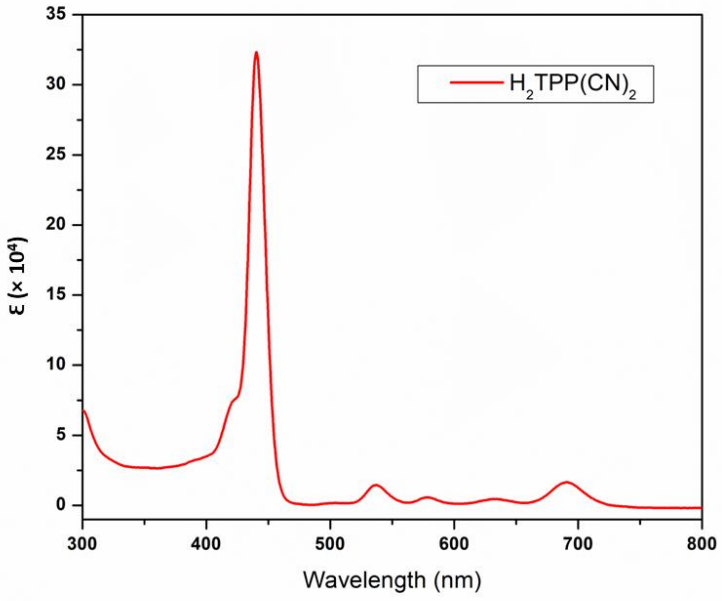
H2TPP(CN)2
ε (× 10^4)
Wavelength (nm)
35
30
25
20
15
10
5
0
300
400
500
600
700
800

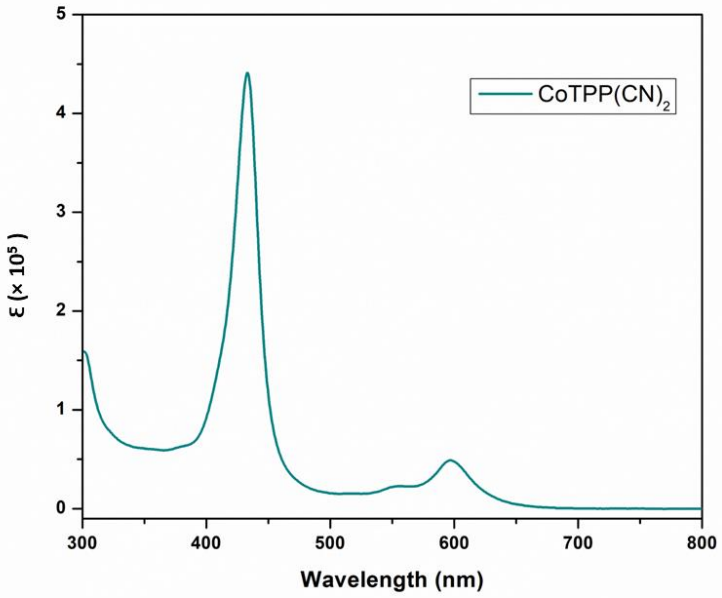
CoTPP(CN)2
ε (× 10⁵)
Wavelength (nm)
0
1
2
3
4
5
300
400
500
600
700
800

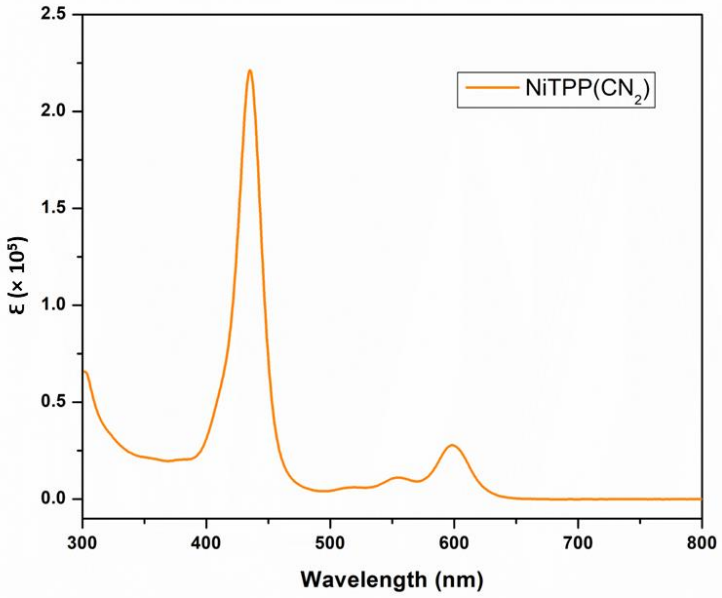
NiTPP(CN2)
ε (× 10⁵)
Wavelength (nm)
0.0
0.5
1.0
1.5
2.0
2.5
300
400
500
600
700
800

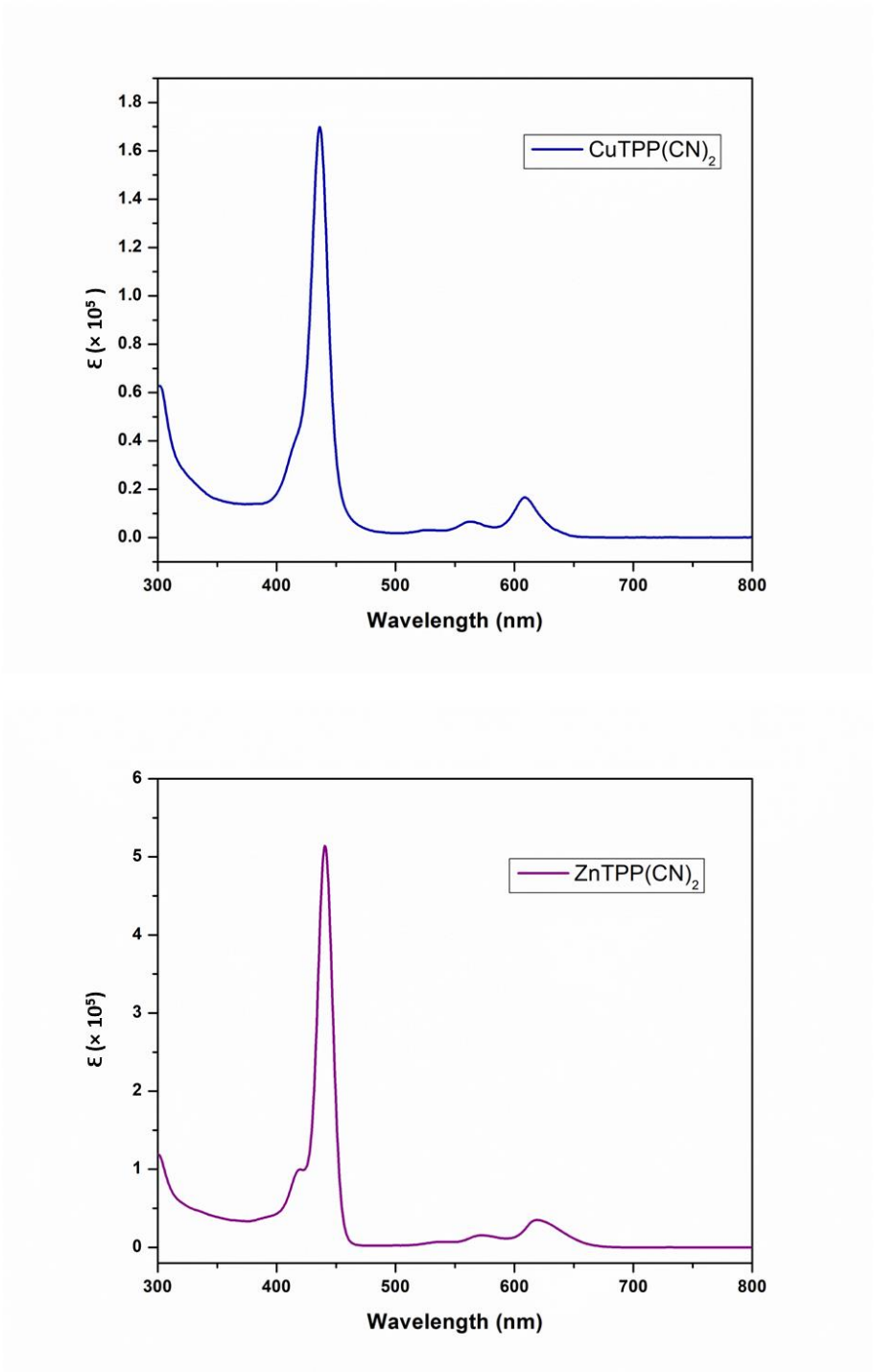

Figure S1. Absorption spectra of MTPP(CN) (M = 2H, Co, Ni Cu and Zn) and MTPP(CN)$_2$ (M = 2H, Co Ni, Cu and Zn) in CH_2Cl_2 at 298K.

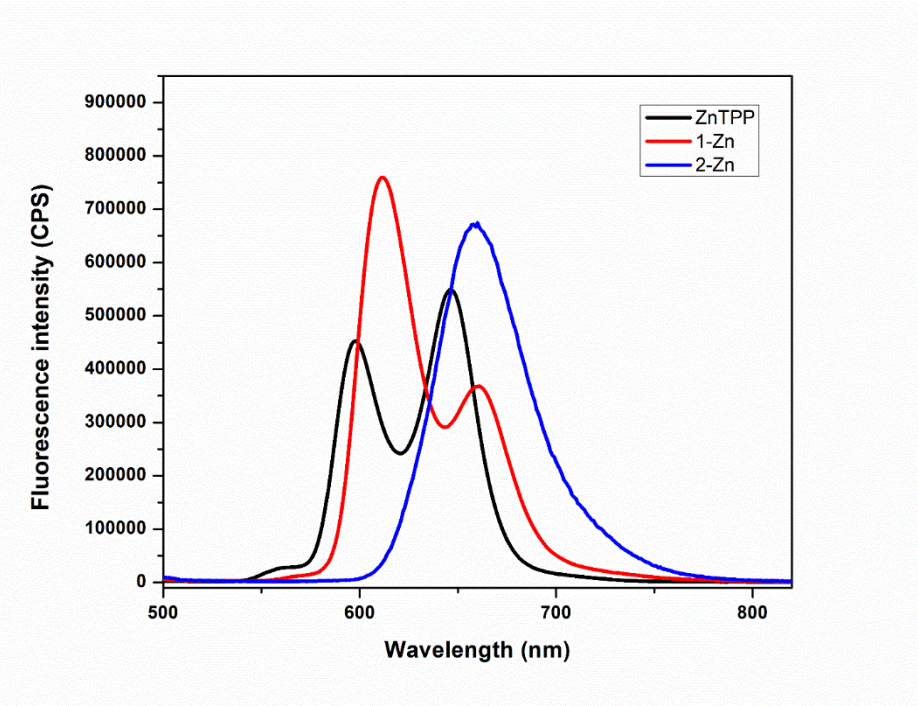

Figure S2. The emission spectra of ZnTPP, ZnTPP(CN)(**1-Zn**), and ZnTPP(CN)$_2$(**2-Zn**) in CH_2Cl_2 at 298 K.

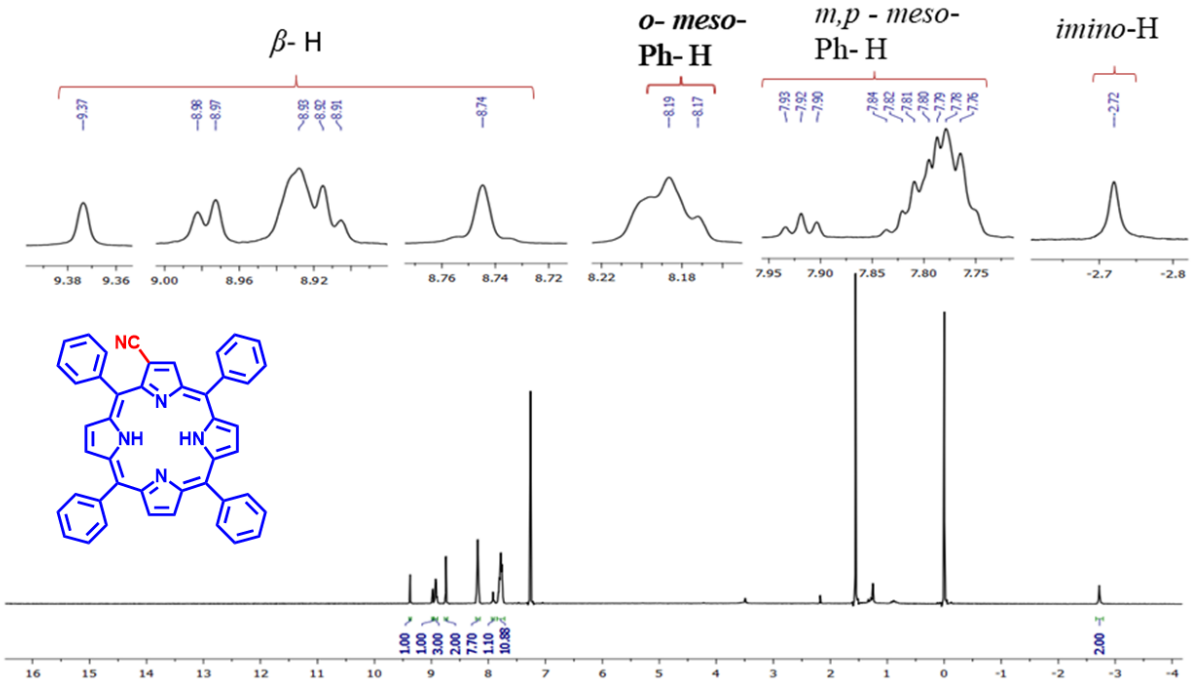

Figure S3. The ^{1}H NMR spectrum of H_2TPP(CN)(**1-H$_2$**) in $CDCl_3$ at 298 K.

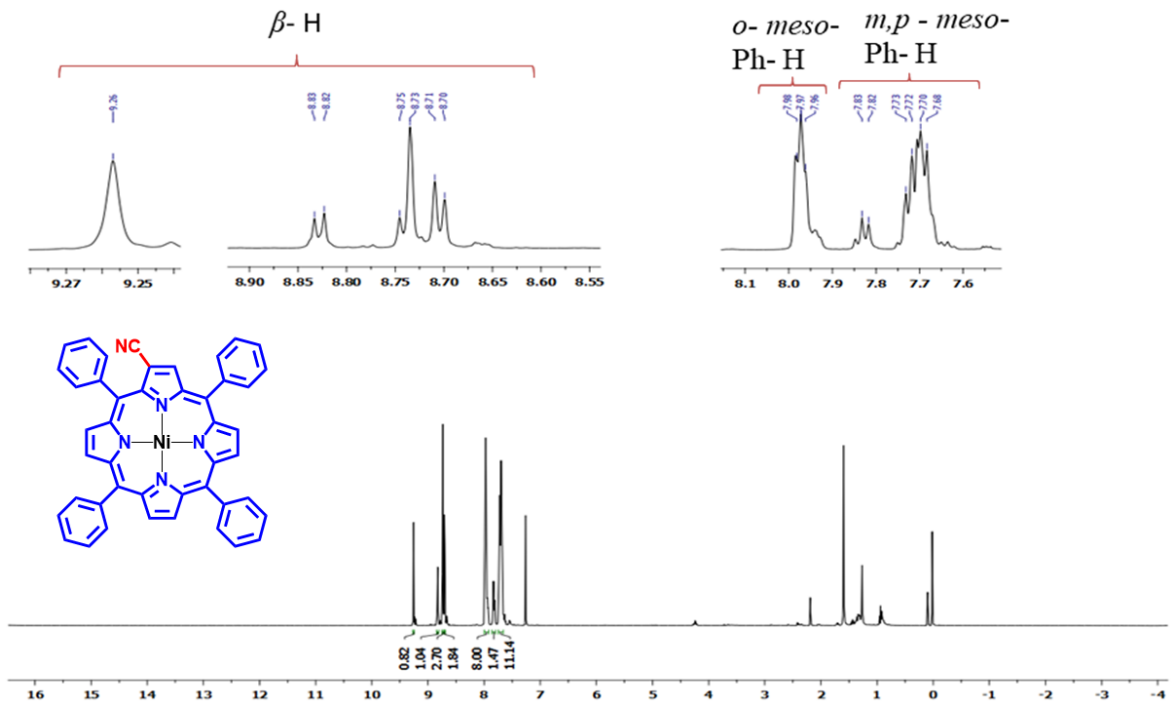

Figure S4. The ^{1}H NMR spectrum of NiTPP(CN)(**1-Ni**) in $CDCl_3$ at 298 K.

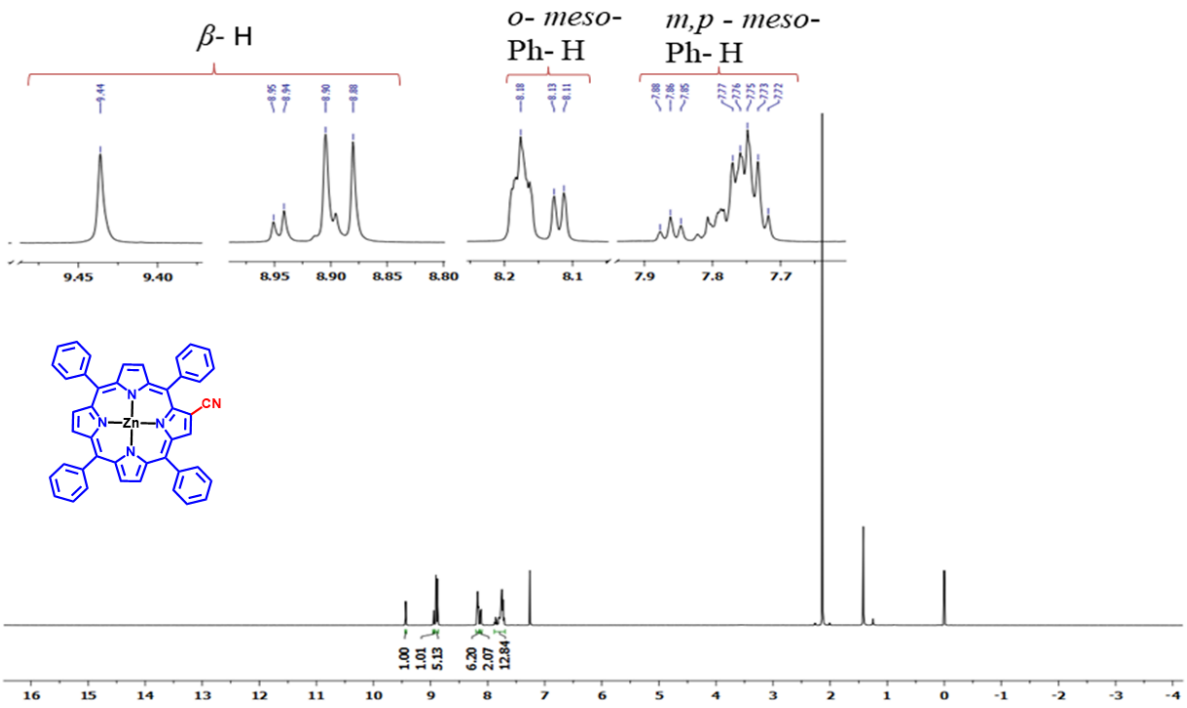

Figure S5. The ^{1}H NMR spectrum of ZnTPP(CN)(**1-Zn**) in $CDCl_3$ at 298 K.

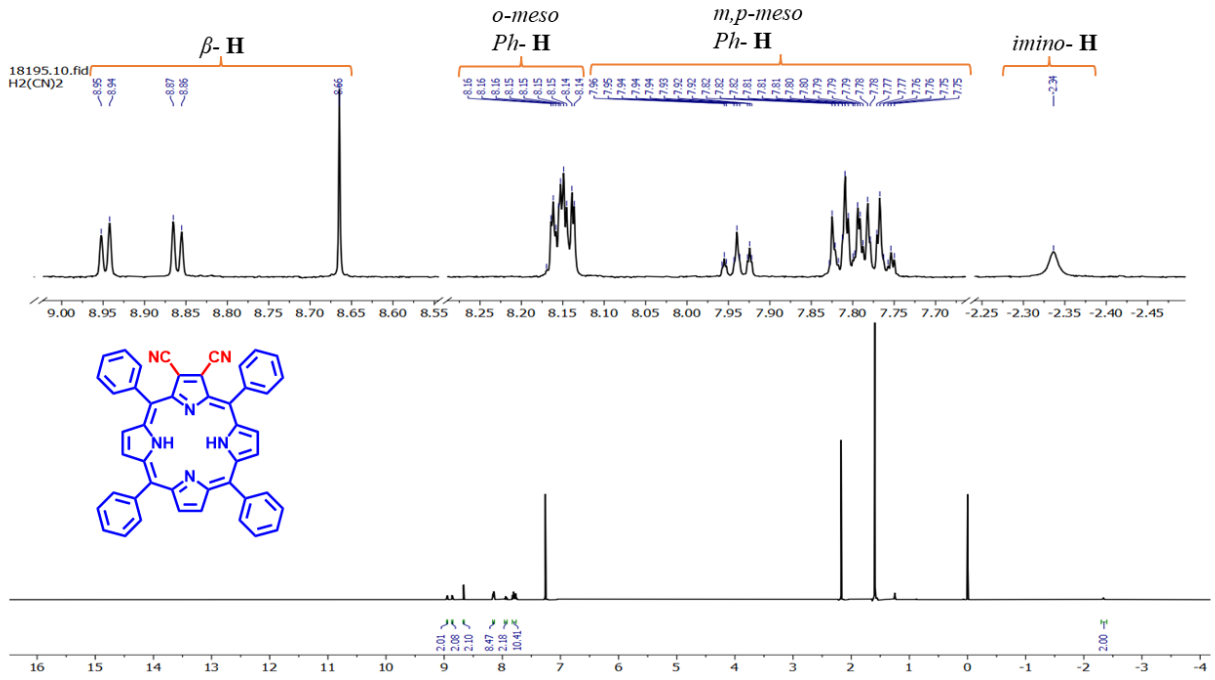

Figure S6. The ^{1}H NMR spectrum of $H_2TPP(CN)_2$(**2-H$_2$**) in $CDCl_3$ at 298 K.

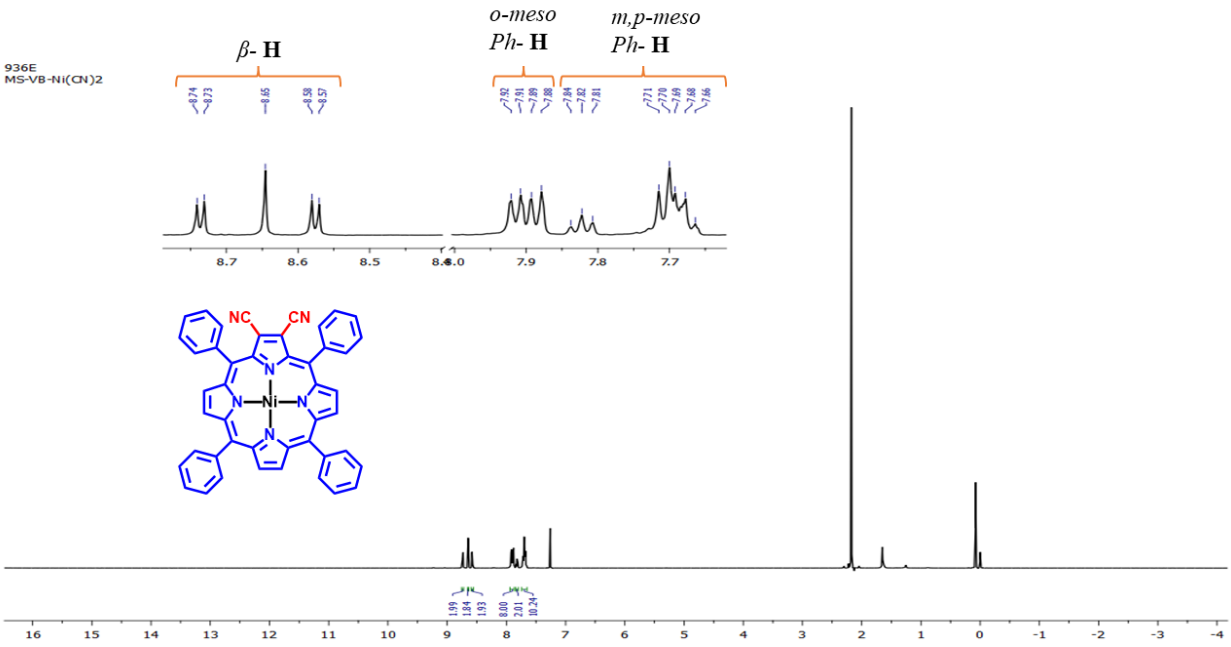

Figure S7. The ^{1}H NMR spectrum of $NiTPP(CN)_2$(**2-Ni**) in $CDCl_3$ at 298 K.

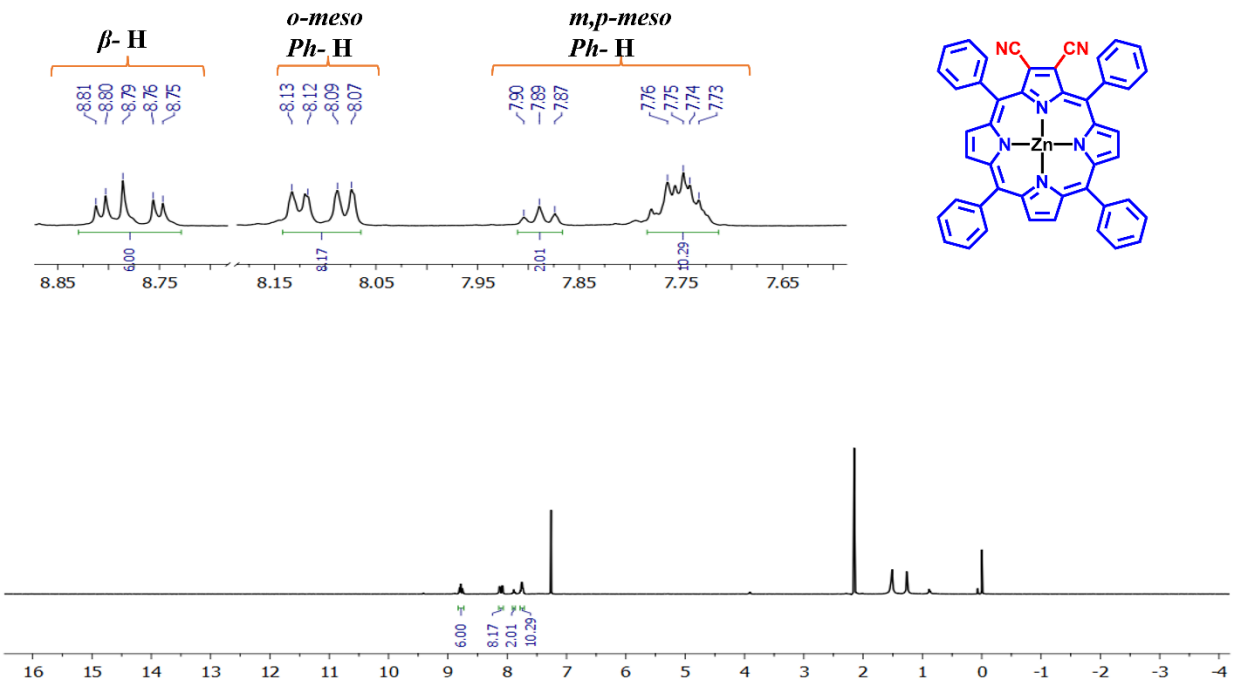

Figure S8. The ^{1}H NMR spectrum of ZnTPP(CN)$_2$(**2-Zn**) in $CDCl_3$ at 298 K.

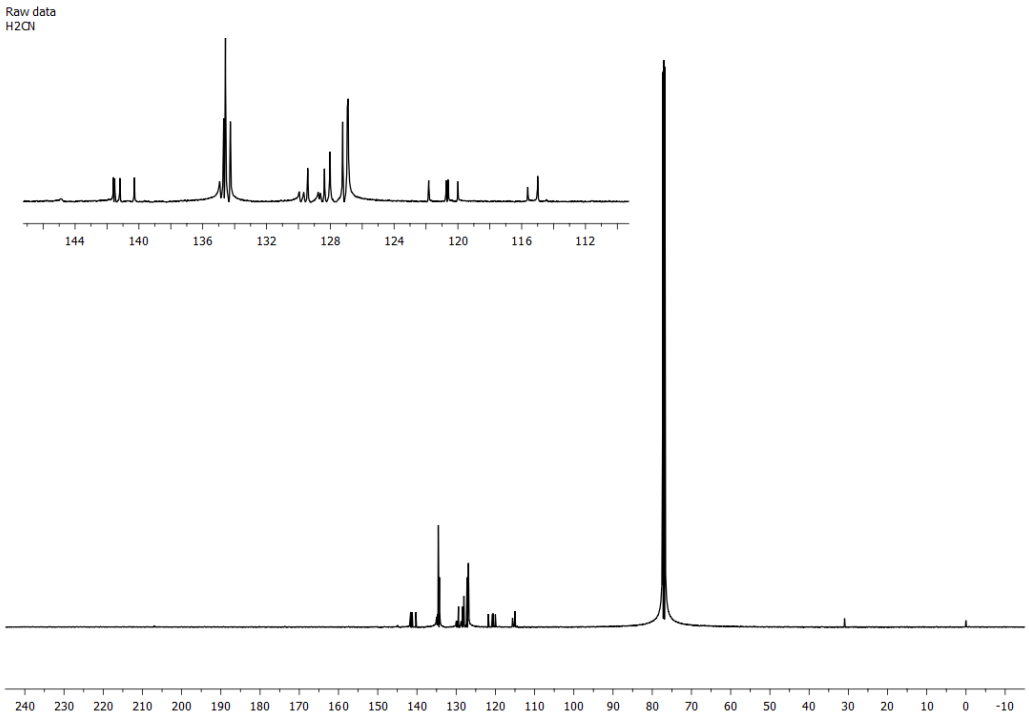

Figure S9. The ^{13} C NMR spectrum of H_2TPP(CN)(**1-H$_2$**) in $CDCl_3$ at 298 K.

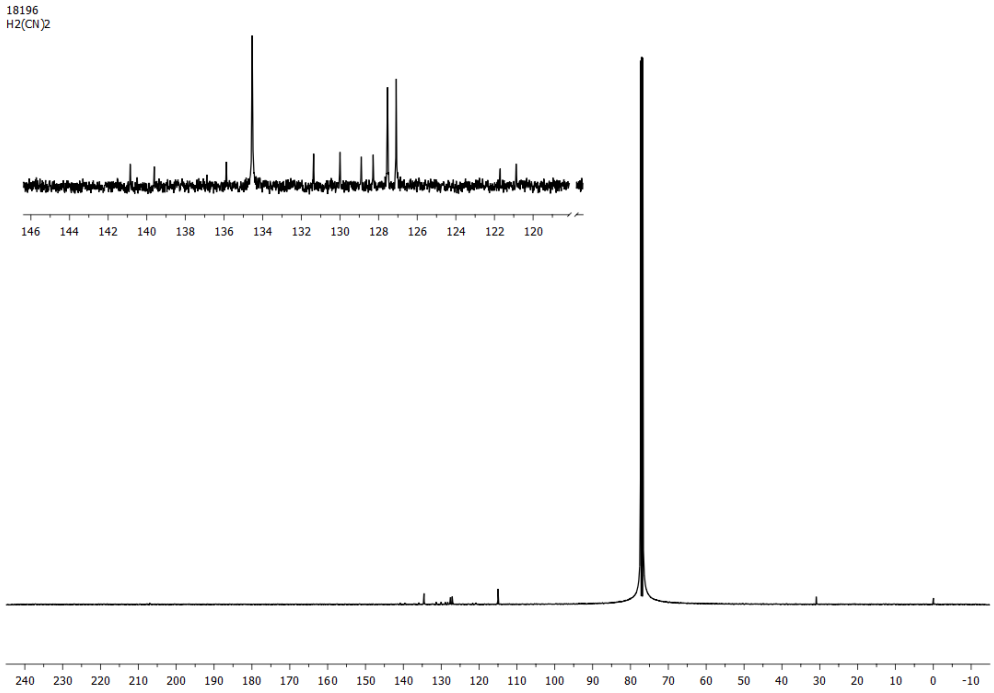

Figure S10. The ^{13} C NMR spectrum of H_2TPP(CN)2(**2- H_2**) in $CDCl_3$ at 298 K.

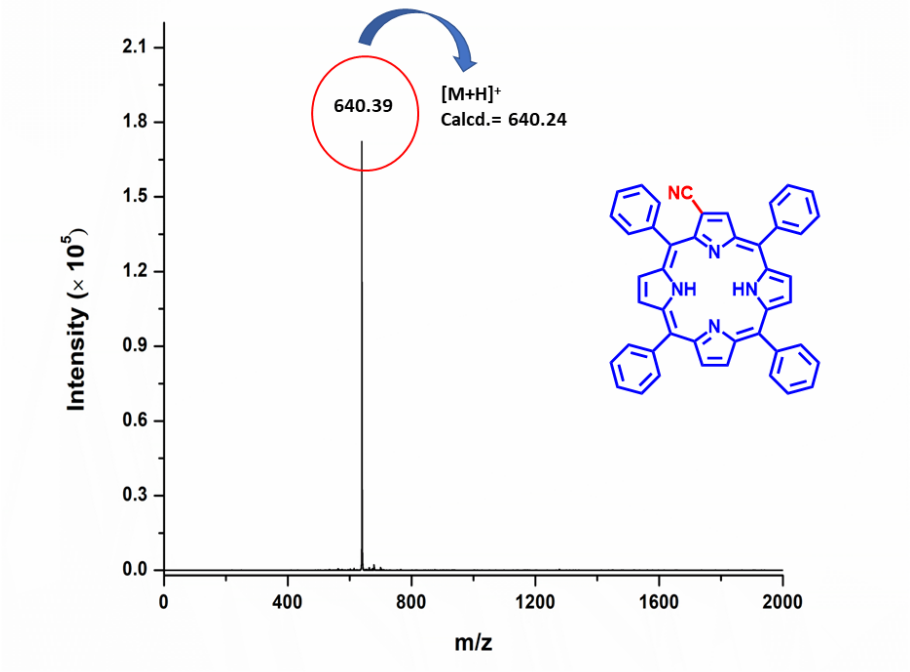

Figure S11. The MALDI-TOF-MS of H_2TPP(CN)(**1-H_2**) in positive ion mode at 298 K.

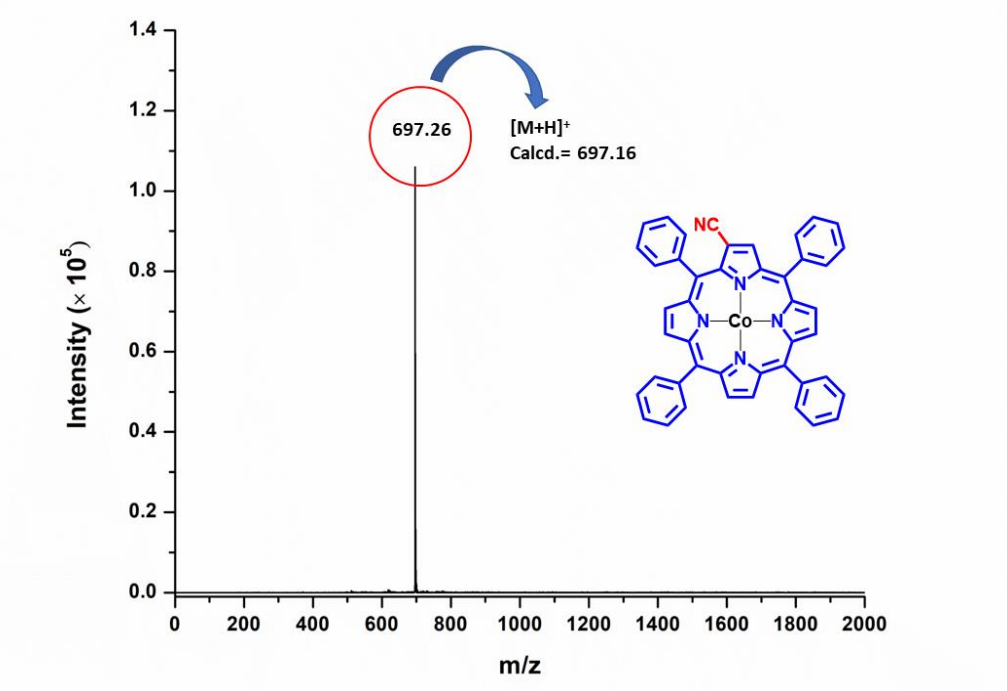

Figure S12. The MALDI-TOF-MS of CoTPP(CN)(**1-Co**) in positive ion mode at 298 K.

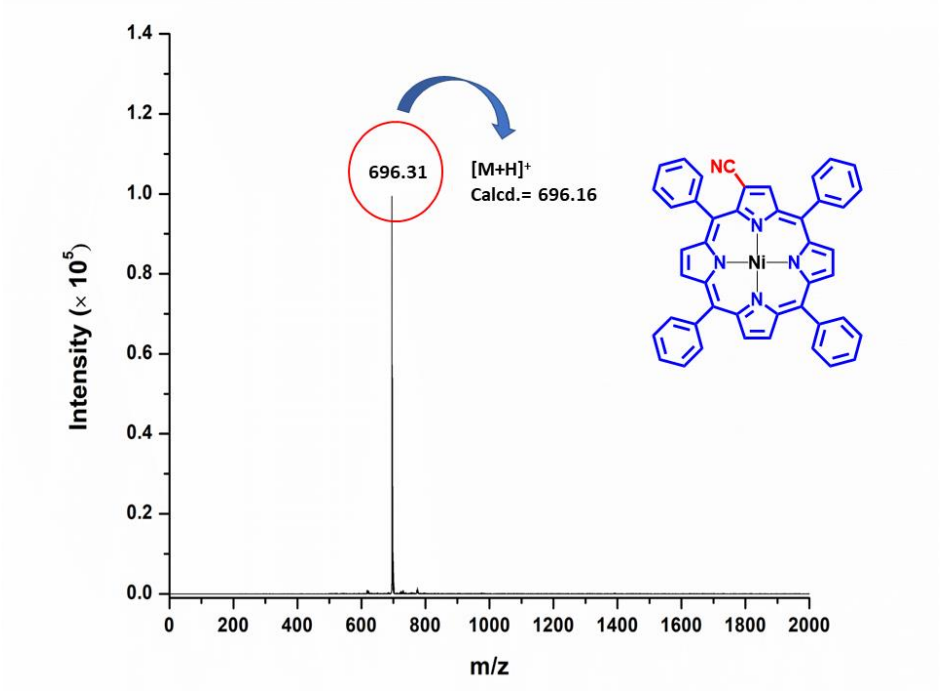

Figure S13. The MALDI-TOF-MS of NiTPP(CN)(**1-Ni**) in positive ion mode at 298 K.

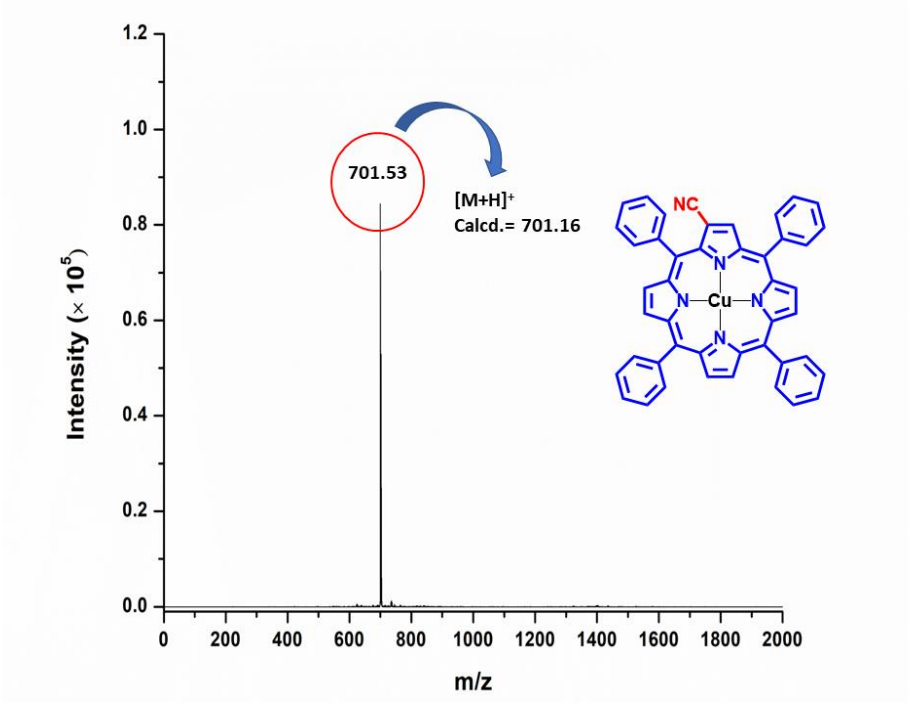

Figure S14. The MALDI-TOF-MS of CuTPP(CN)(**1-Cu**) in positive ion mode at 298 K.

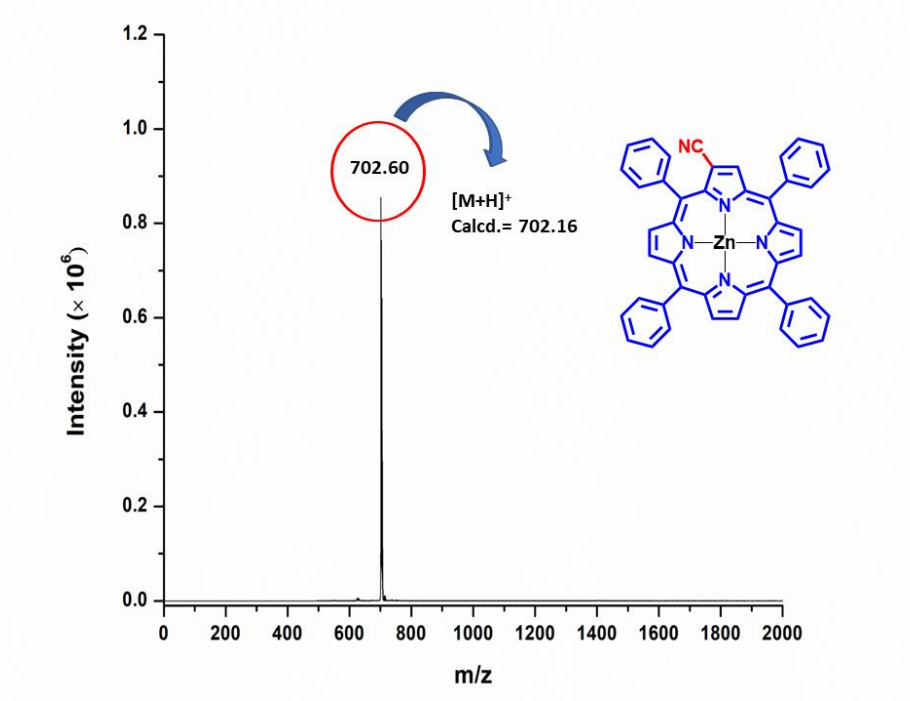

Figure S15. The MALDI-TOF-MS of ZnTPP(CN)(**1-Zn**) in positive ion mode at 298 K.

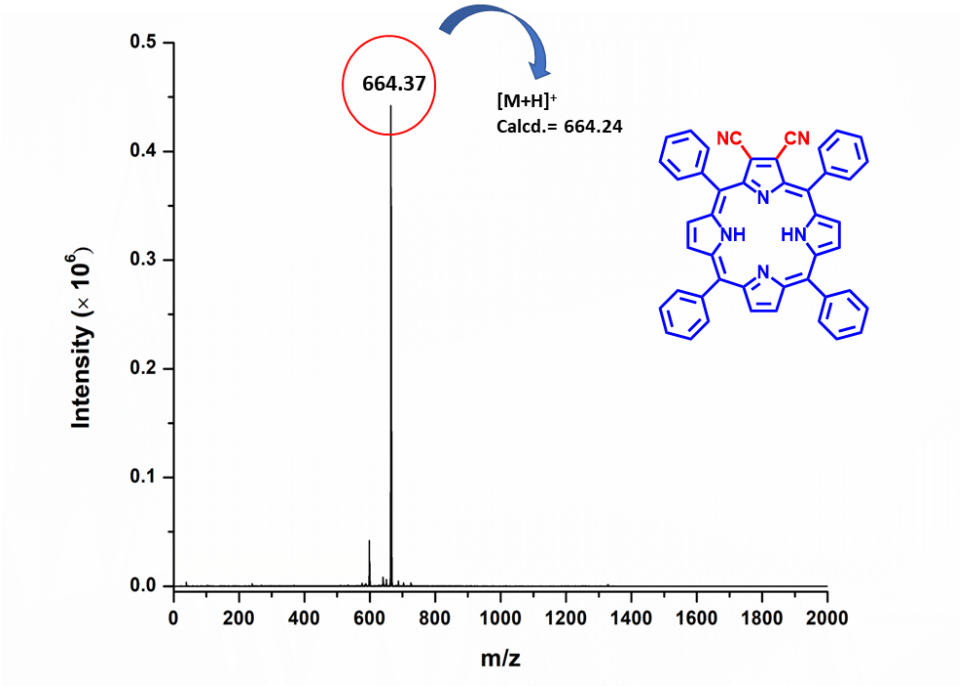

Figure S16. The MALDI-TOF-MS of $H_2TPP(CN)_2$(**2-H$_2$**) in positive ion mode at 298 K.

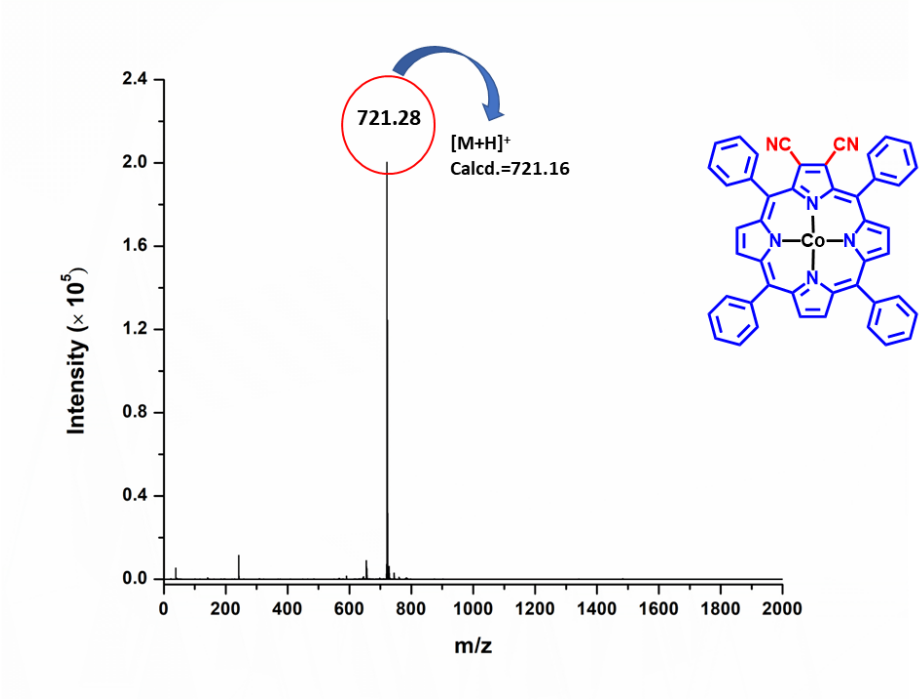

Figure S17. The MALDI-TOF-MS of $CoTPP(CN)_2$(**2-Co**) in positive ion mode at 298 K.

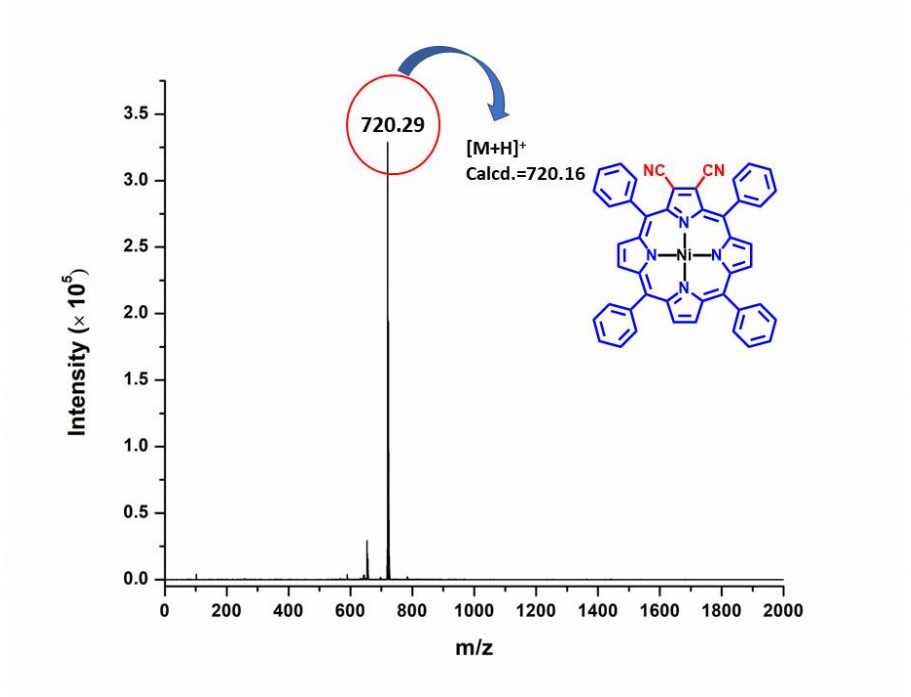

Figure S18. The MALDI-TOF-MS of NiTPP(CN)$_2$(**2-Ni**) in positive ion mode at 298 K.

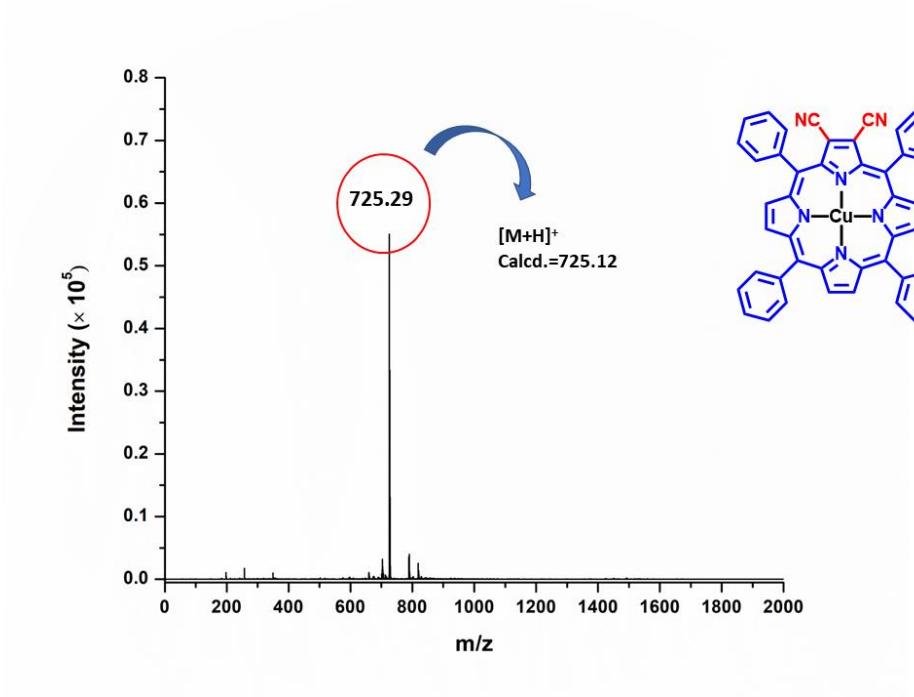

Figure S19. The MALDI-TOF-MS of CuTPP(CN)$_2$(**2-Cu**) in positive ion mode at 298 K.

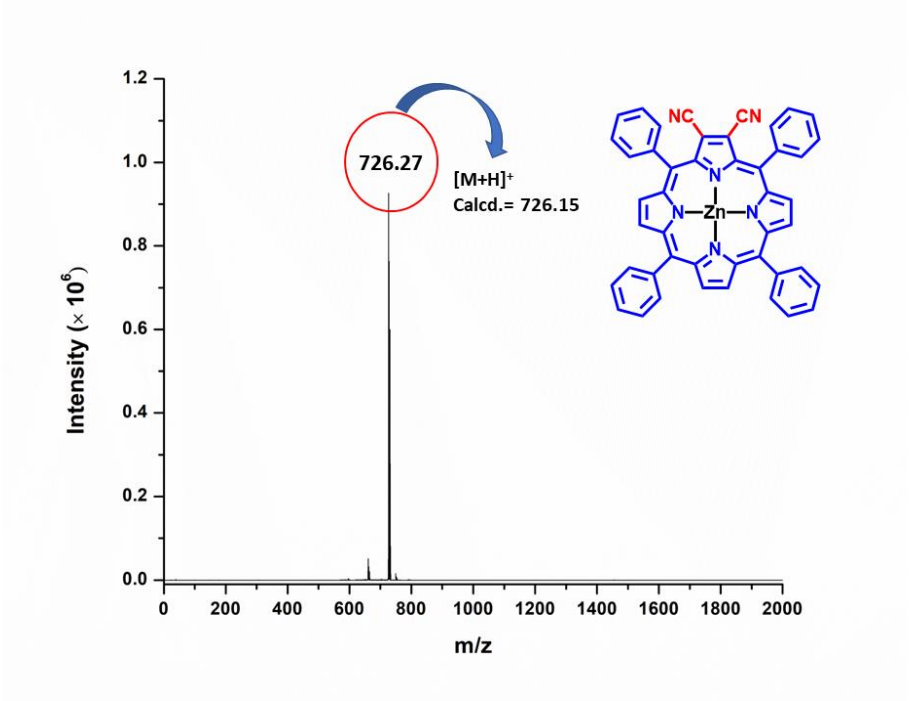

Figure S20. The MALDI-TOF-MS of $ZnTPP(CN)_2$(**2-Zn**) in positive ion mode at 298 K.

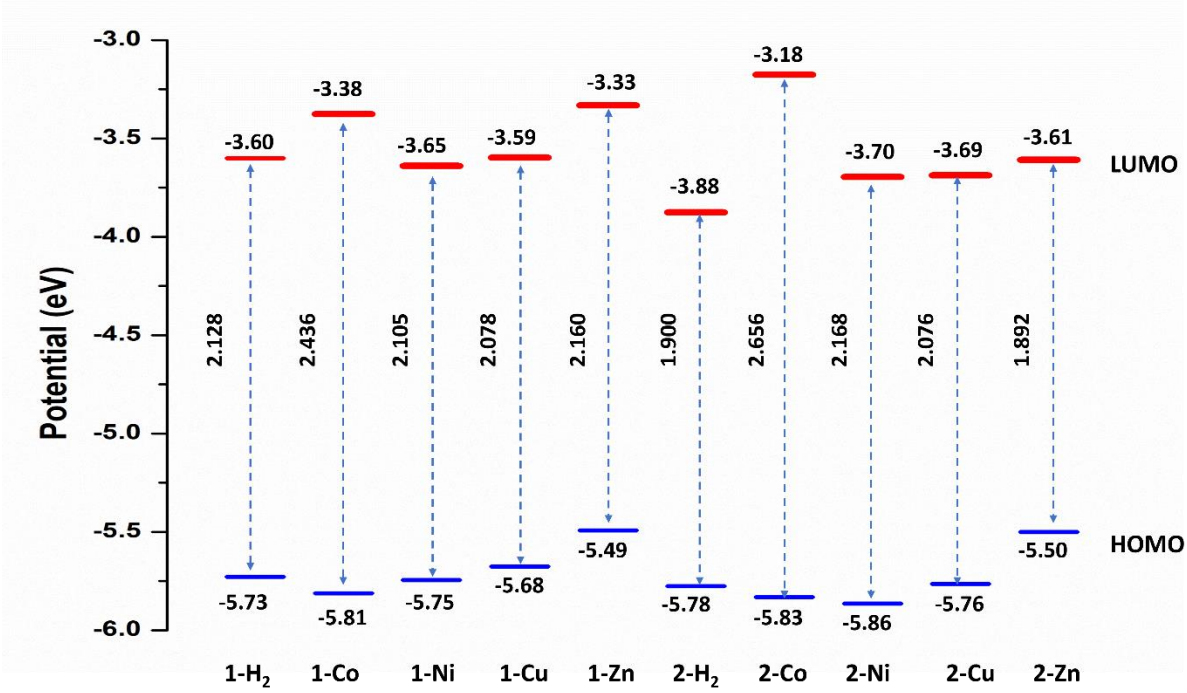

Figure S21. The HOMO-LUMO energies of the porphyrins calculated from electrochemical data.

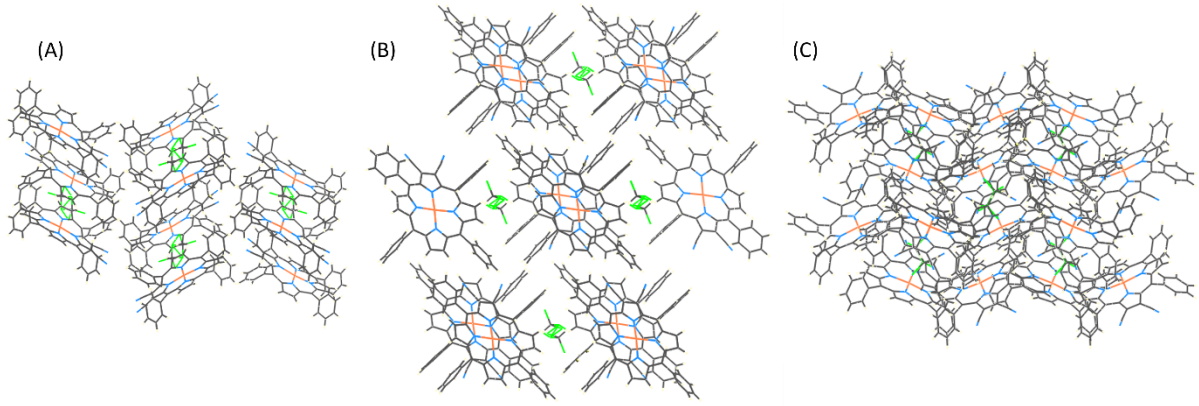

Figure S22. The Crystal structure arrangement along (a) a-axis, (b) b-axis, and (c) c-axis. (Trapped solvent molecules are shown in between).

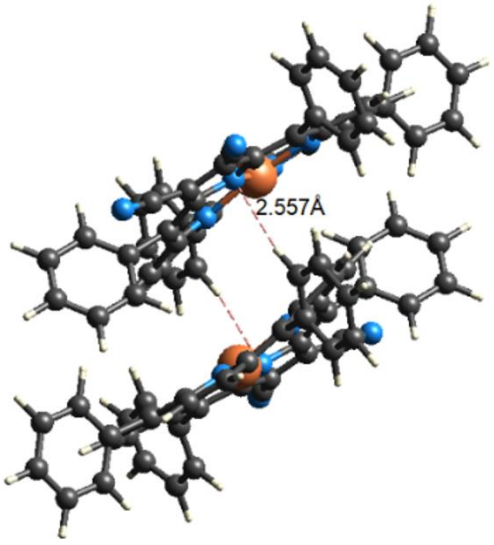

Figure S23. The H-bonding (inner N----H) Interaction in crystal packing.

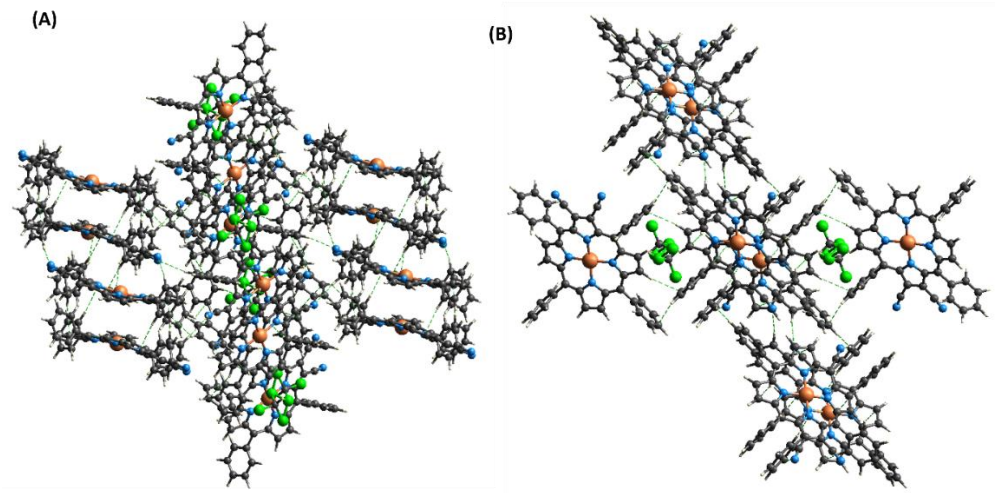

Figure S24. Role of Hydrogen interactions in crystal packing arrangements as shown in different orientations.

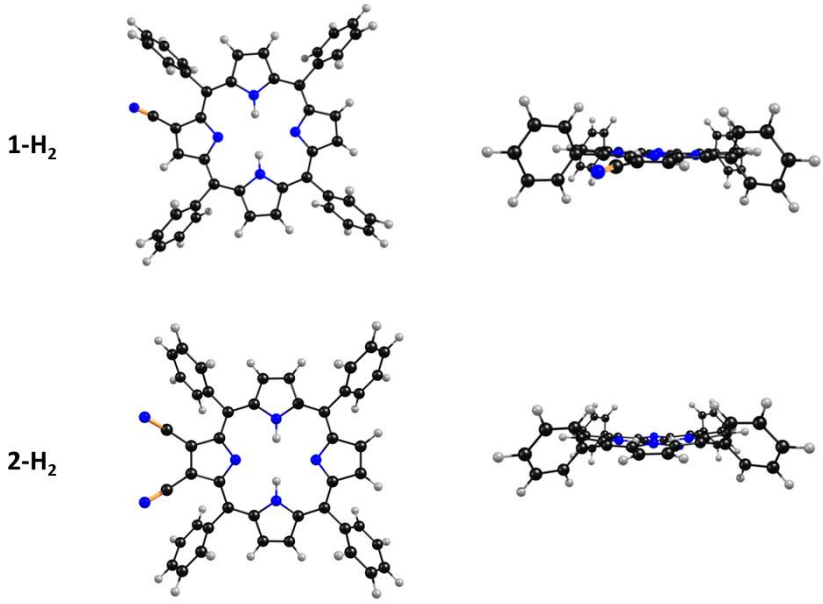

Figure S25. Ground state optimized geometries of $H_2TPP(CN)_2$(**2-H$_2$**) and $H_2TPP(CN)$(**1-H$_2$**) using B3LYP as functional set and LANL2DZ as the basis set. Left side: top view and right side: side view.

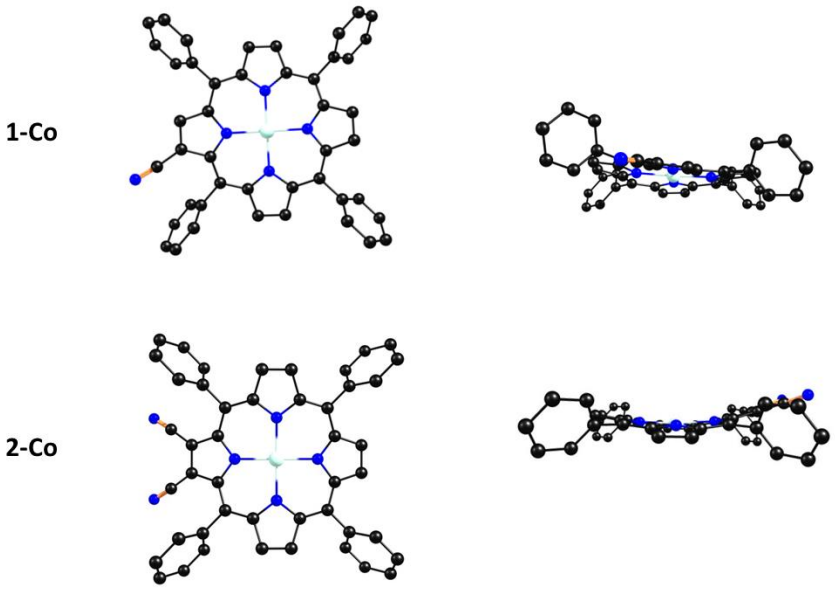

Figure S26. Ground state optimized geometries of CoTPP(CN)$_2$(**2-Co**) and CoTPP(CN)(**1-Co**) using B3LYP as functional set and LANL2DZ as the basis set. Left side: top view and right side: side view.

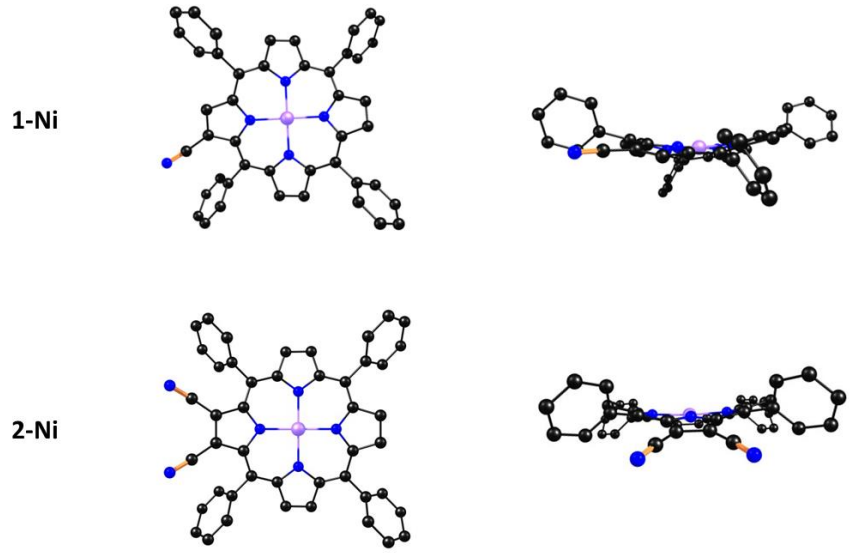

Figure S27. Ground state optimized geometries of NiTPP(CN)$_2$(**2-Ni**) and NiTPP(CN)(**1-Ni**) using B3LYP as functional set and LANL2DZ as the basis set. Left side: top view and right side: side view.

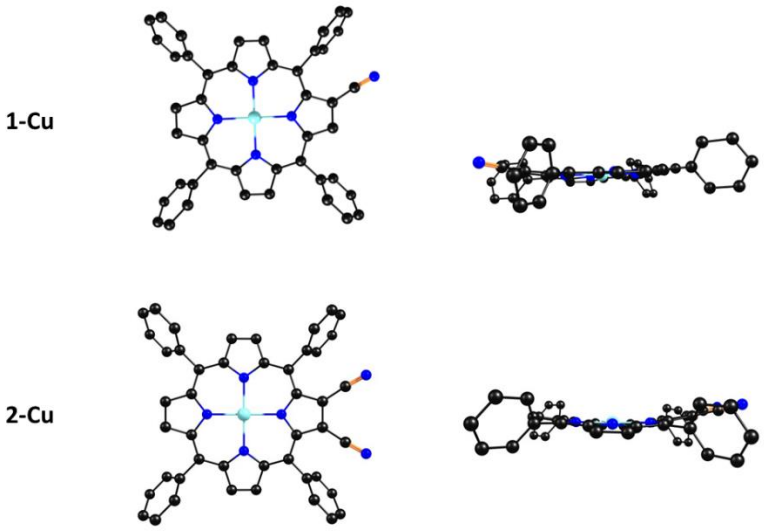

Figure S28. Ground state optimized geometries of CuTPP(CN)$_2$(**2-Cu**) and CuTPP(CN)(**1-Cu**) using B3LYP as functional set and LANL2DZ as the basis set. Left side: top view and right side: side view.

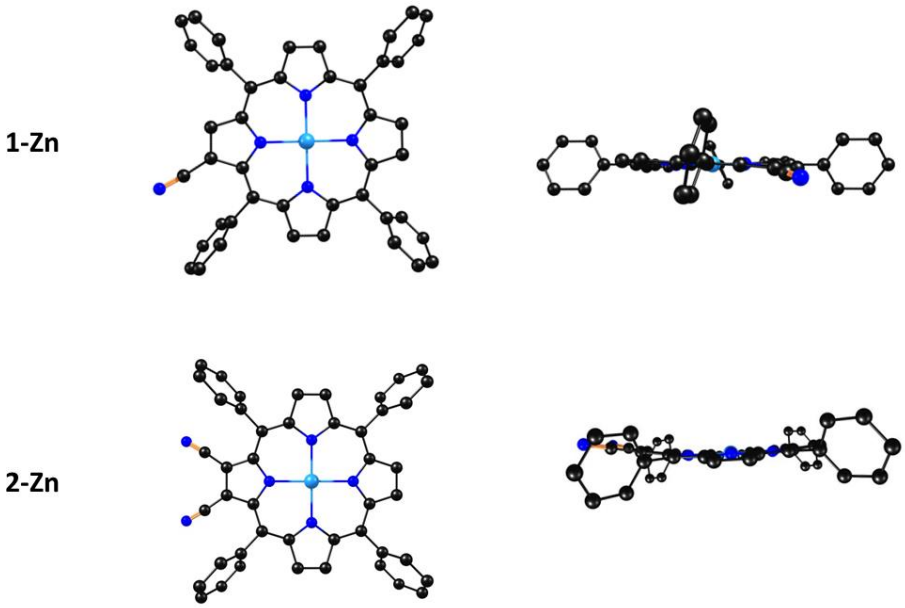

Figure S29. Ground state optimized geometries of ZnTPP(CN)$_2$(**2-Zn**) and ZnTPP(CN)(**1-Zn**) using B3LYP as functional set and LANL2DZ as the basis set. Left side: top view and right side: side view.

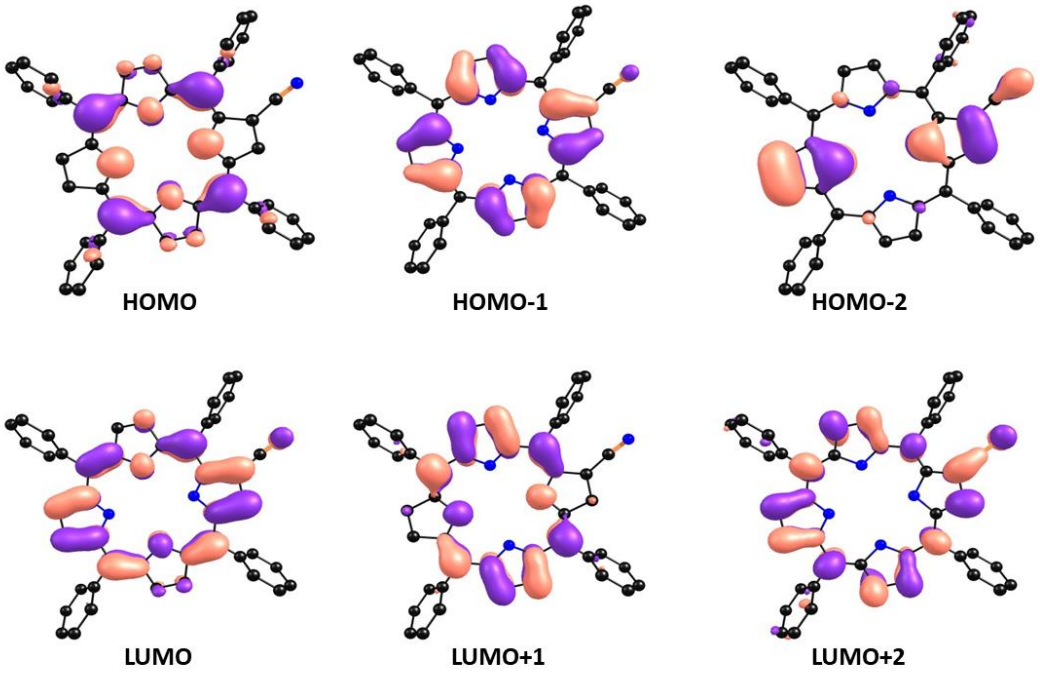

Figure S30. Frontier molecular orbitals of H_2TPP(CN)(**1-H$_2$**).

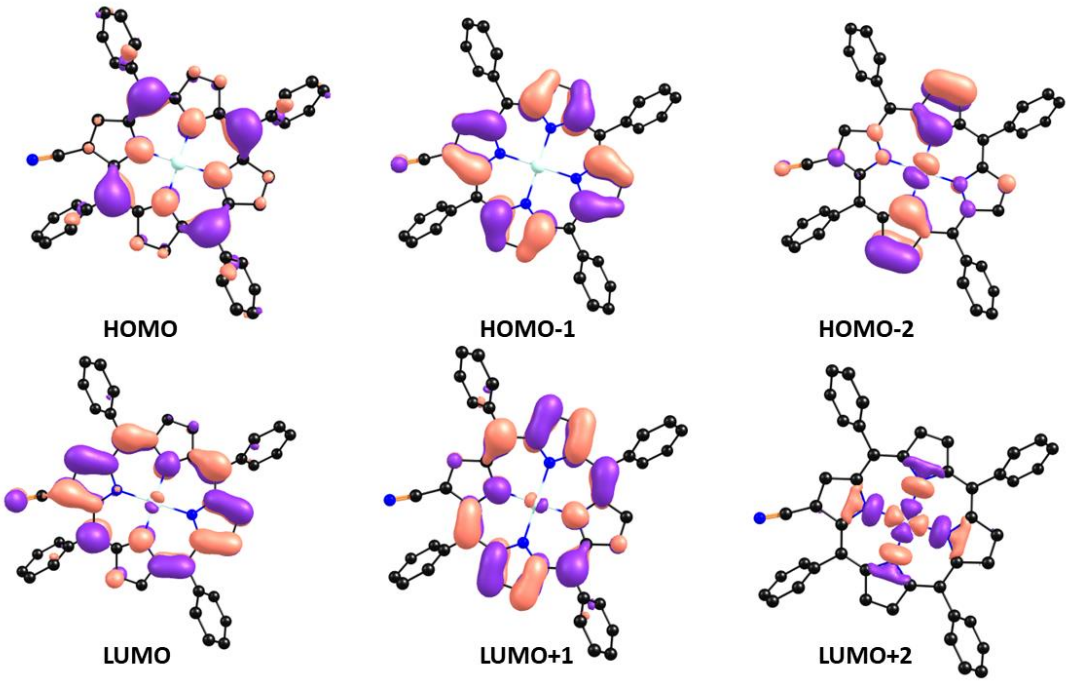

Figure S31. Frontier molecular orbitals of CoTPP(CN)(**1-Co**).

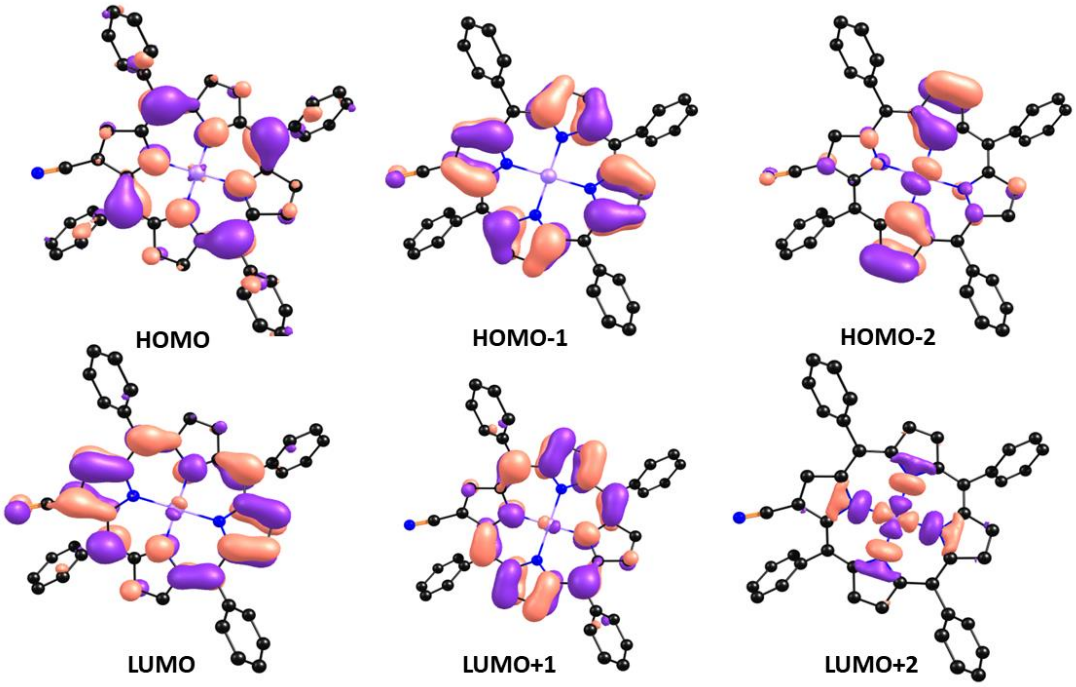

Figure S32. Frontier molecular orbitals of NiTPP(CN)(**1-Ni**).

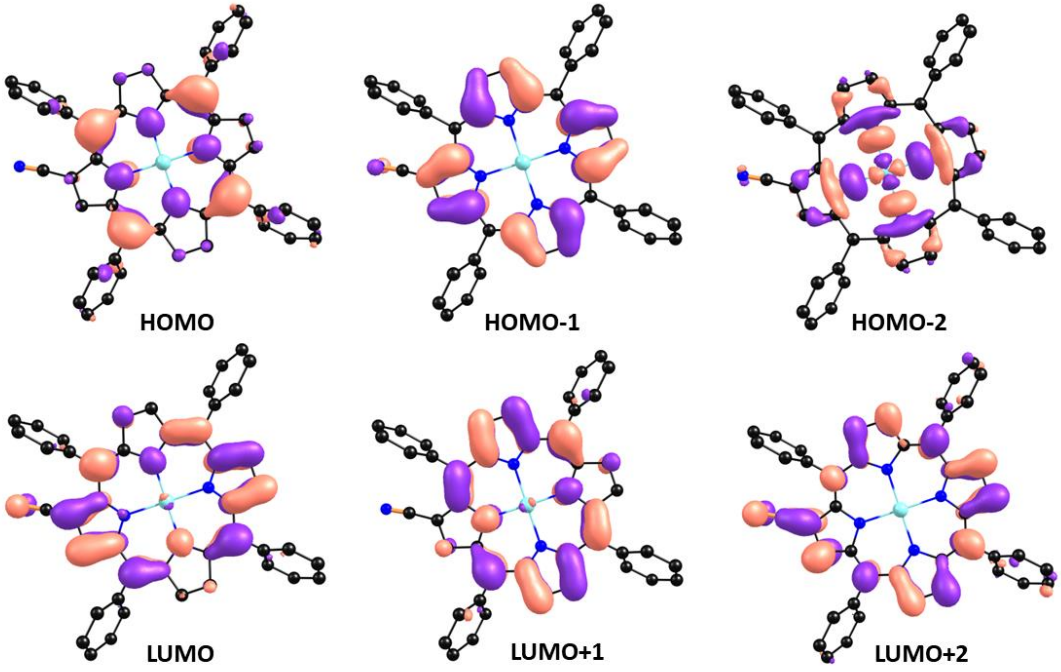

Figure S33. Frontier molecular orbitals of CuTPP(CN)(**1-Cu**).

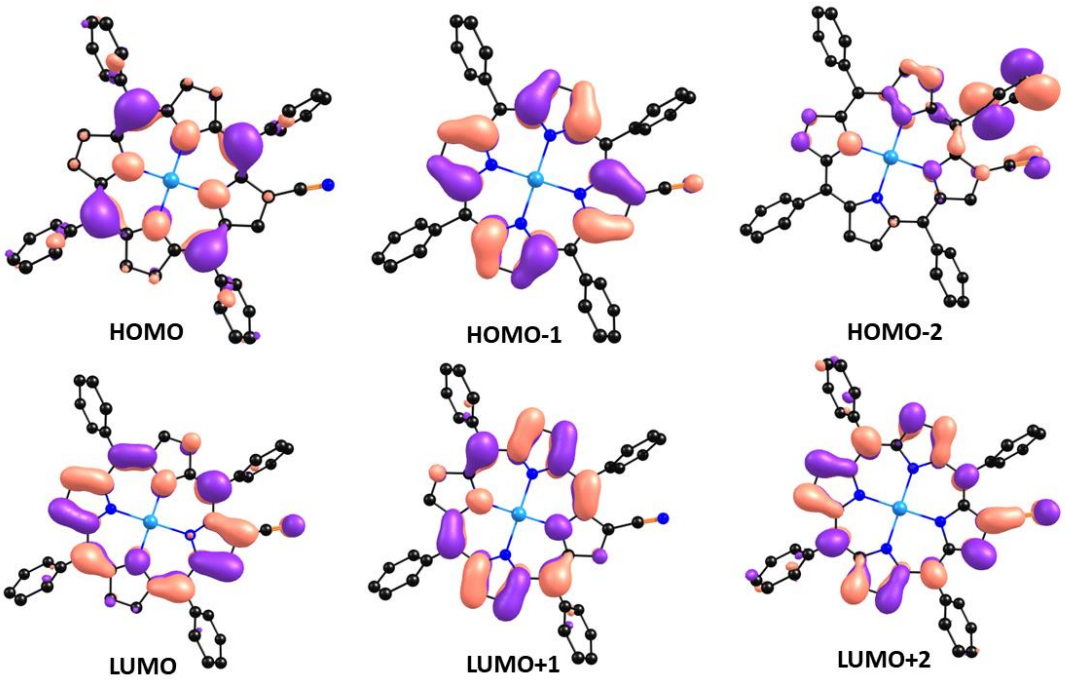

Figure S34. Frontier molecular orbitals of ZnTPP(CN)(**1-Zn**).

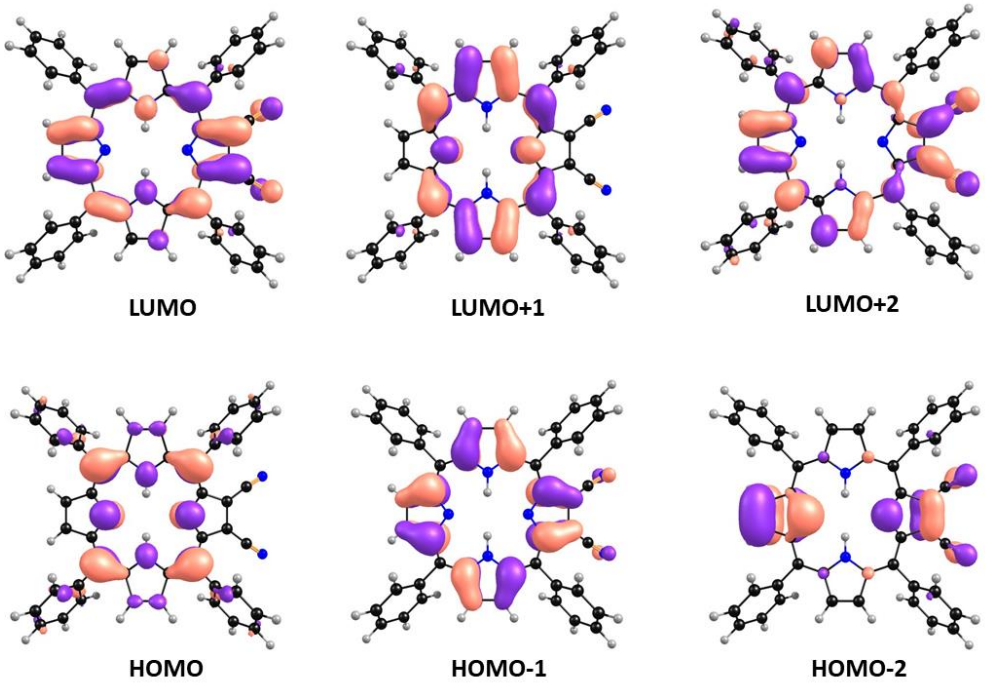

Figure S35. Frontier molecular orbitals of $H_2TPP(CN)_2$(**2-H_2**).

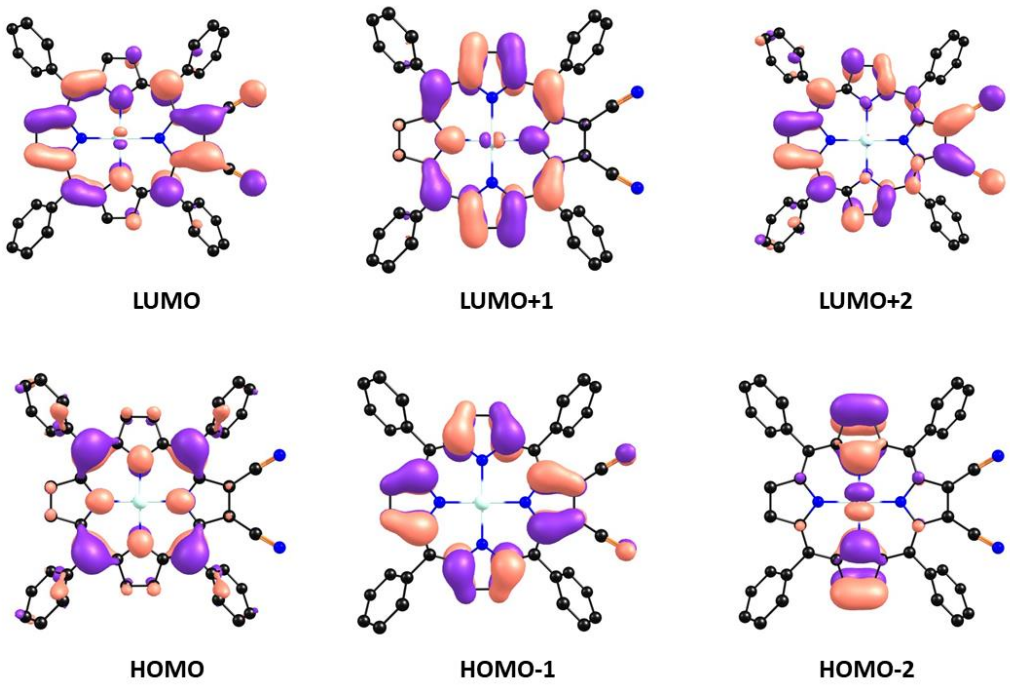

Figure S36. Frontier molecular orbitals of $CoTPP(CN)_2$(**2-Co**).

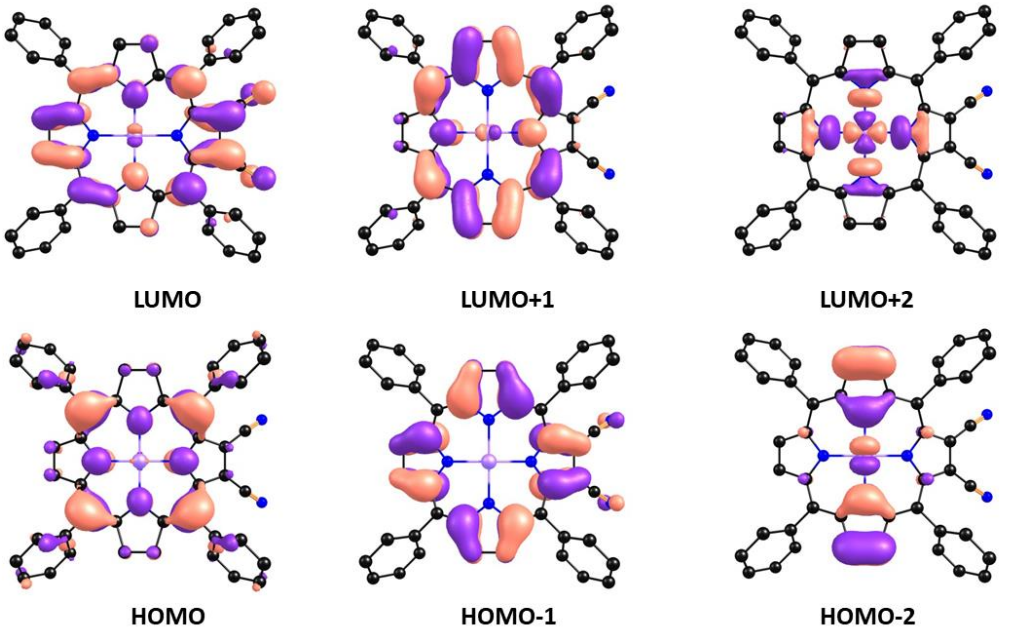

Figure S37. Frontier molecular orbitals of $NiTPP(CN)_2$(**2-Ni**).

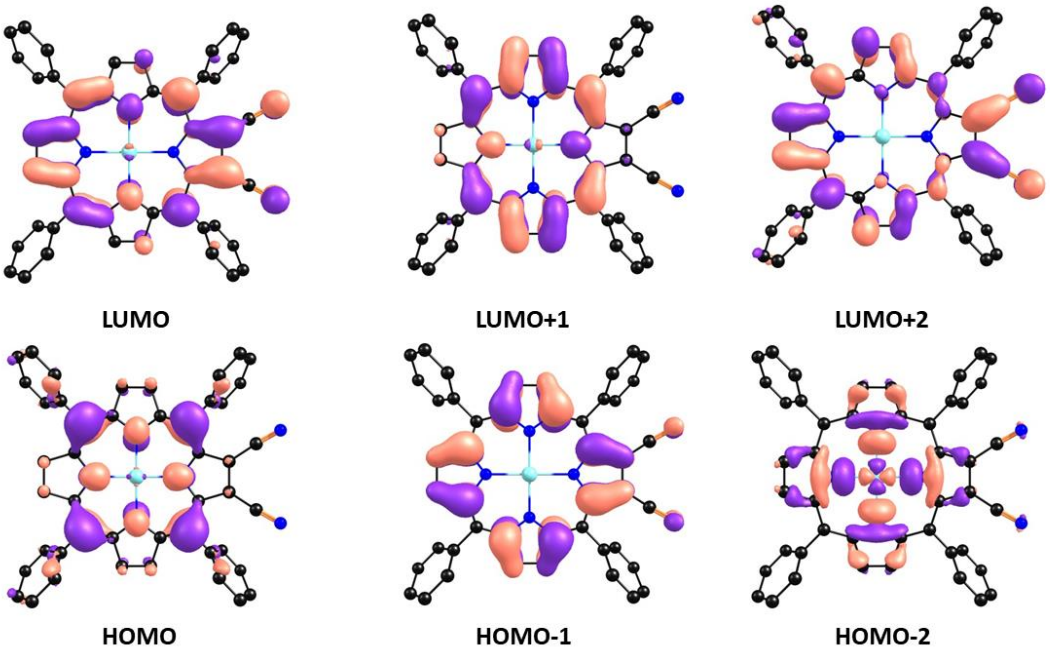

Figure S38. Frontier molecular orbitals of CuTPP(CN)$_2$(**2-Cu**).

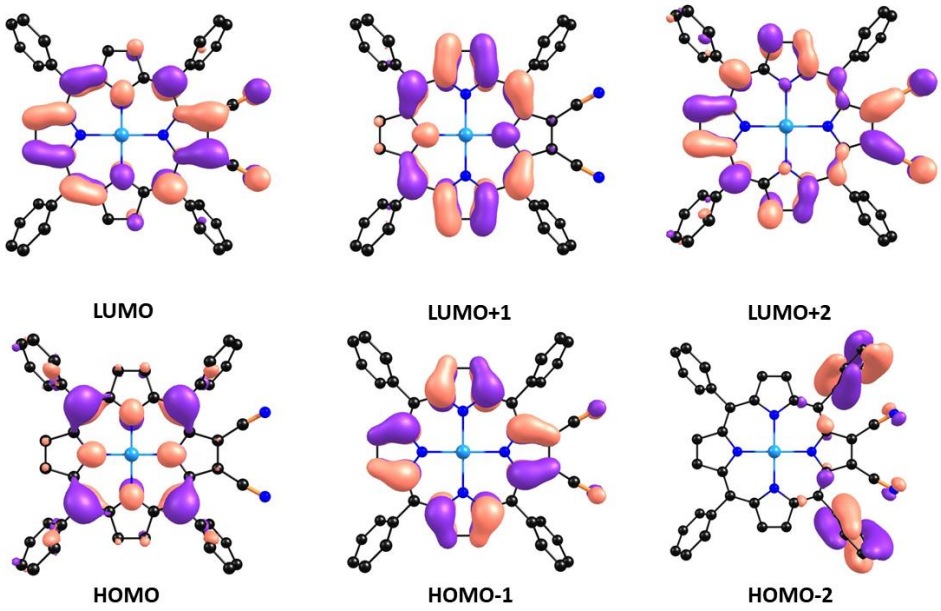

Figure S39. Frontier molecular orbitals of ZnTPP(CN)$_2$(**2-Zn**).

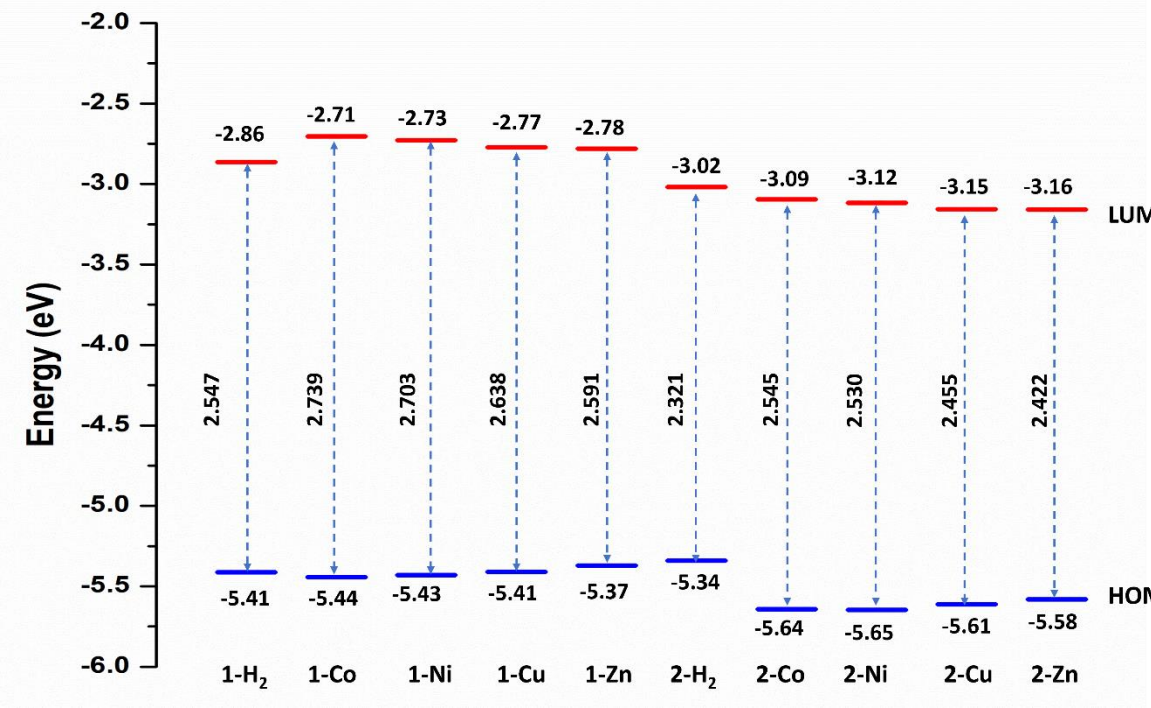

Figure S40. The HOMO-LUMO energies of the porphyrins calculated form DFT calculation.

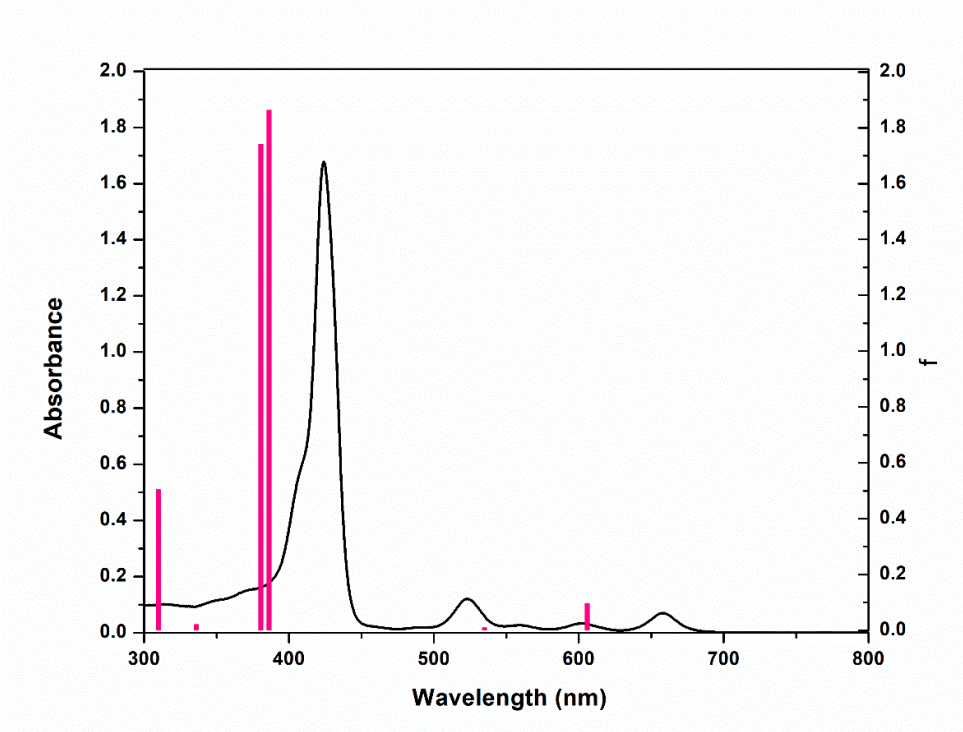

Figure S41. Calculated excitations (pink vertical lines) and experimental absorption spectra (black curve) for **1-H_2**.

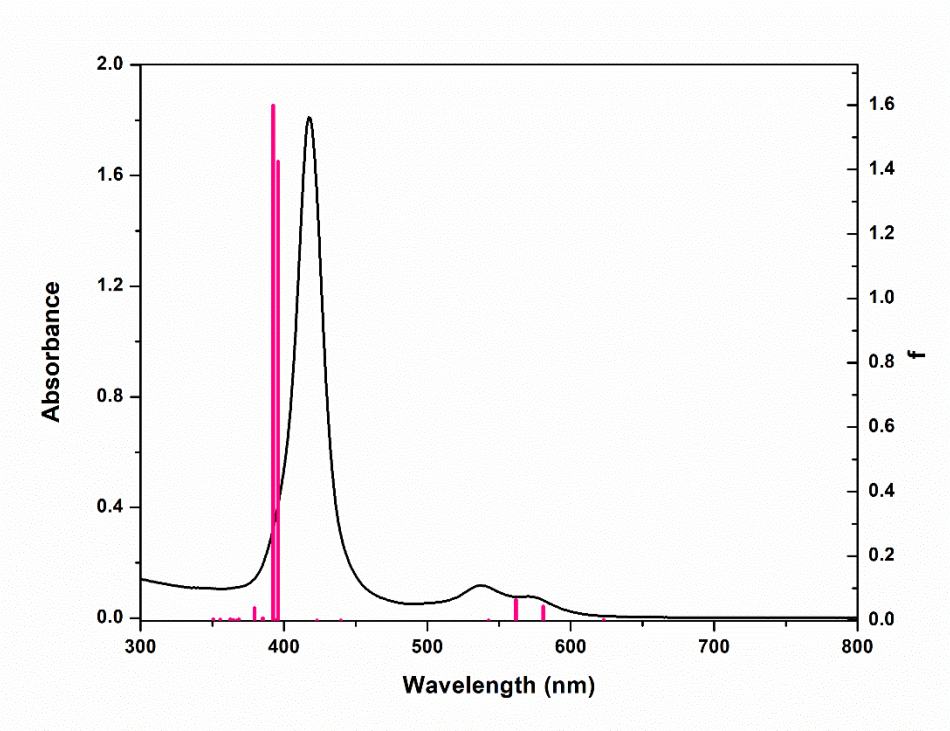

Figure S42. Calculated excitations (pink vertical lines) and experimental absorption spectra (black curve) for **1-Co**.

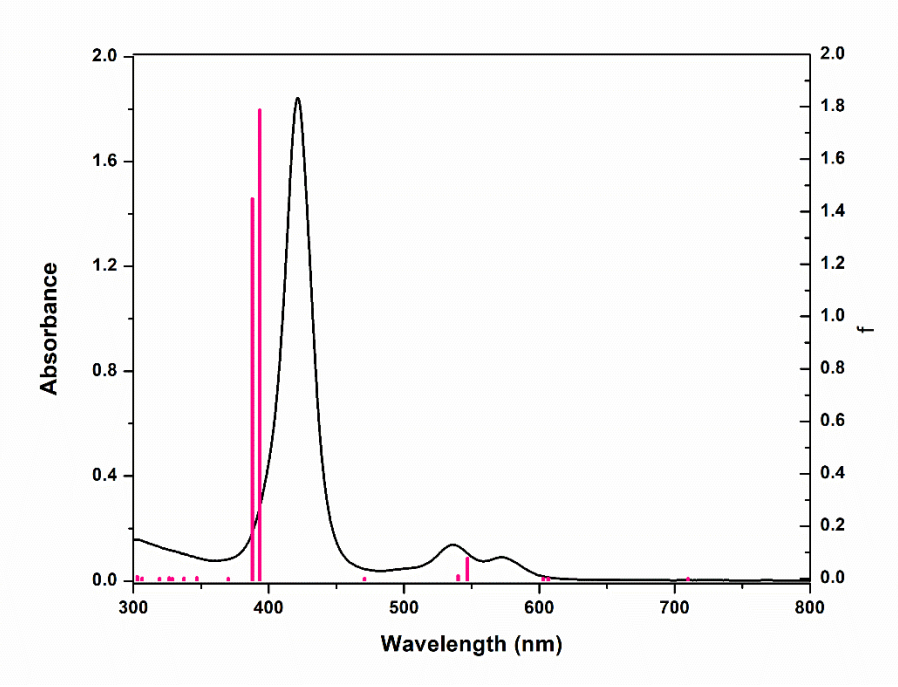

Figure S43. Calculated excitations (pink vertical lines) and experimental absorption spectra (black curve) for **1-Ni**.

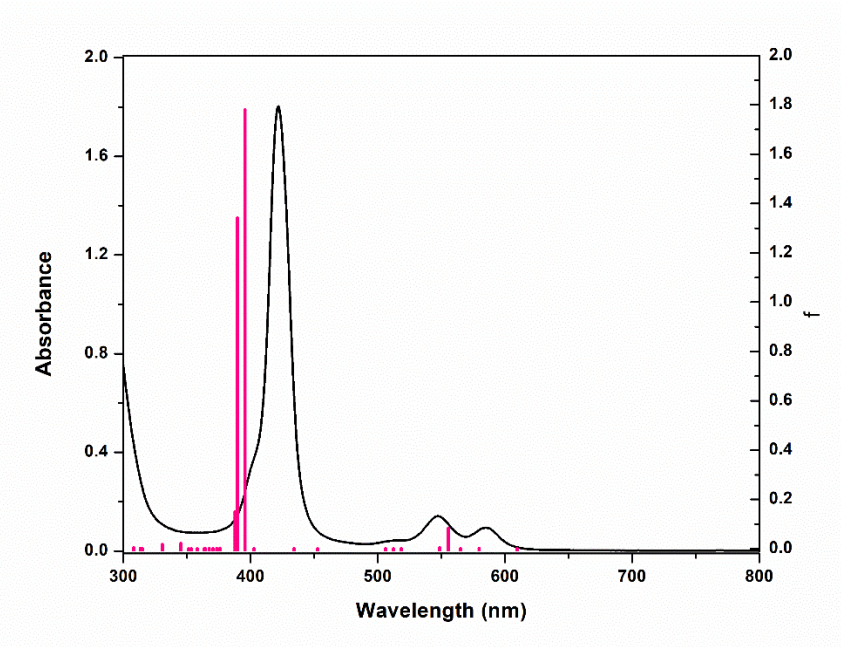

Figure S44. Calculated excitations (pink vertical lines) and experimental absorption spectra (black curve) for **1-Cu**.

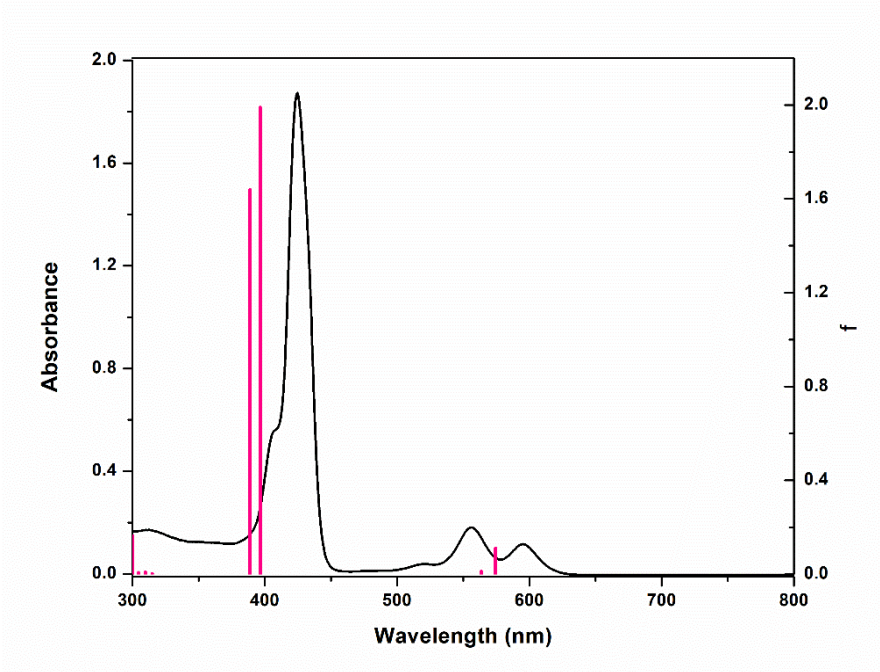

Figure S45. Calculated excitations (pink vertical lines) and experimental absorption spectra (black curve) for **1-Zn**.

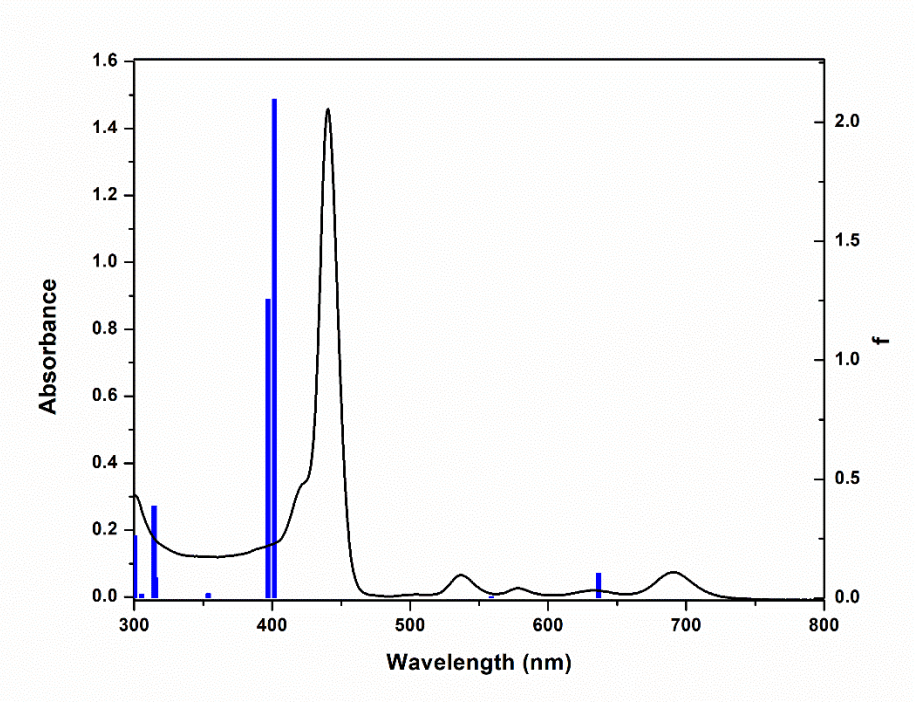

Figure S46. Calculated excitations (blue vertical lines) and experimental absorption spectra (black curve) for **2-H_2**.

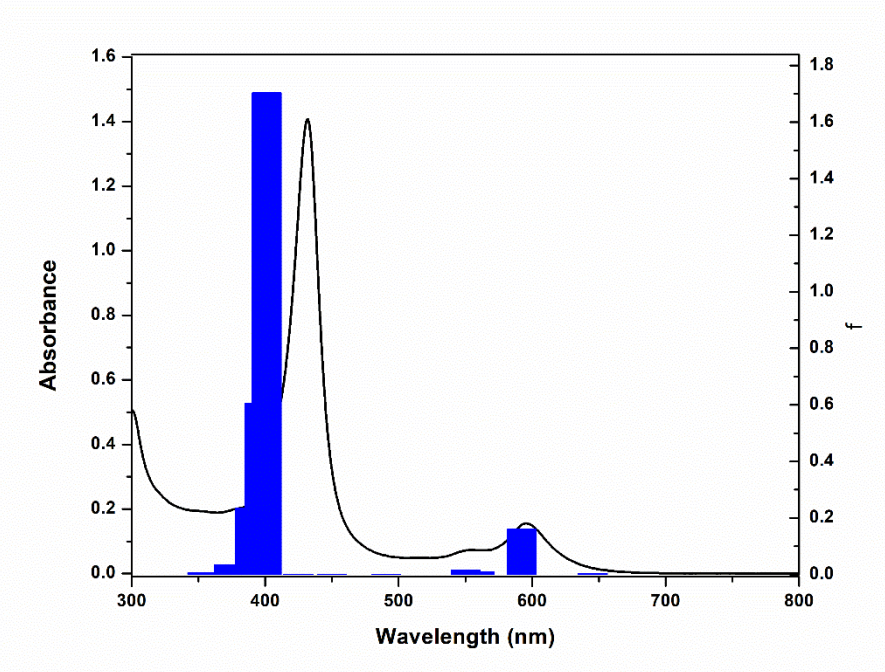

Figure S47. Calculated excitations (blue vertical lines) and experimental absorption spectra (black curve) for **2-Co**.

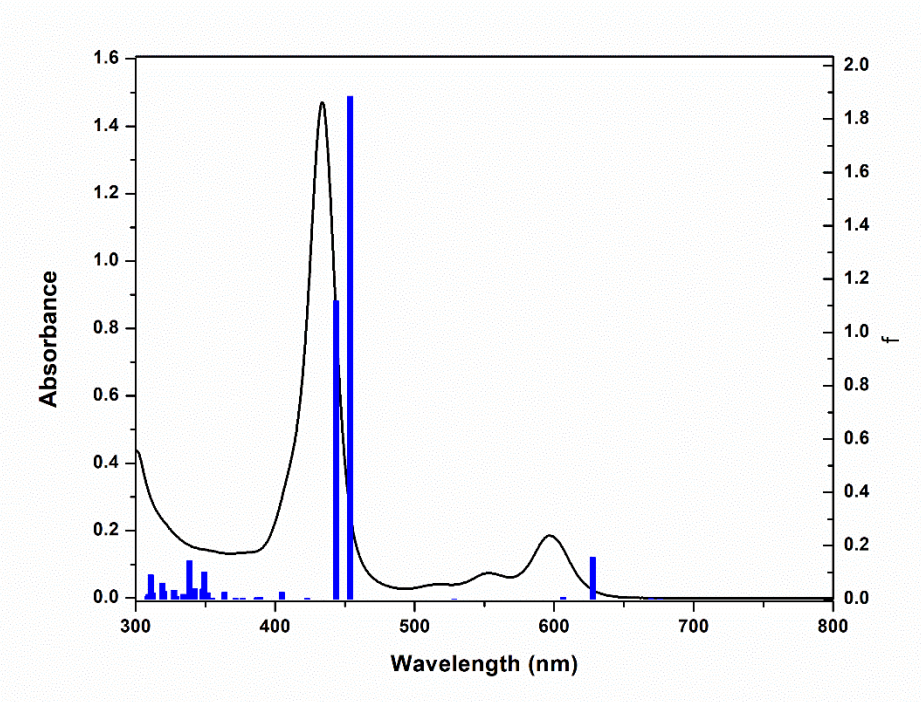

Figure S48. Calculated excitations (blue vertical lines) and experimental absorption spectra (black curve) for **2-Ni**.

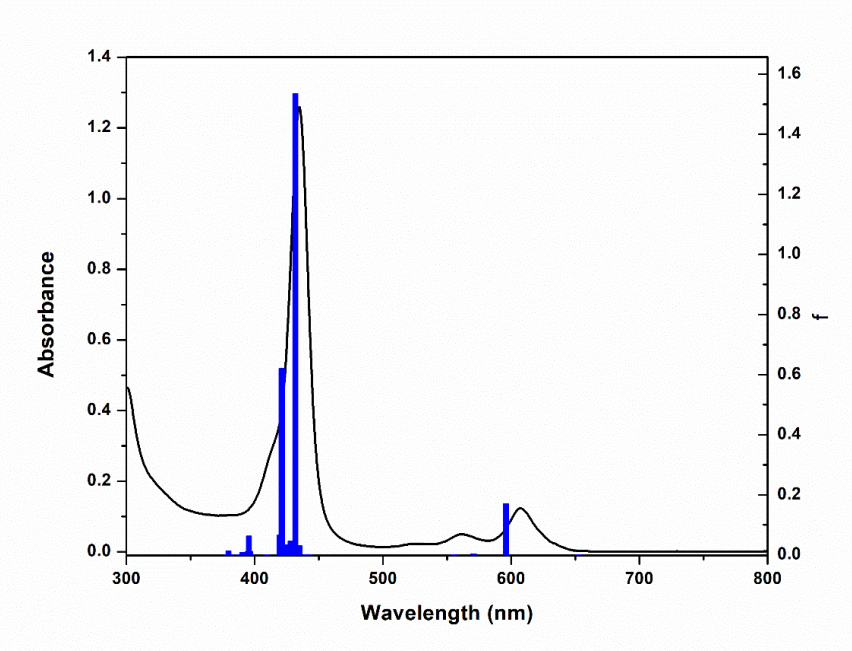

Figure S49. Calculated excitations (blue vertical lines) and experimental absorption spectra (black curve) for **2-Cu**.

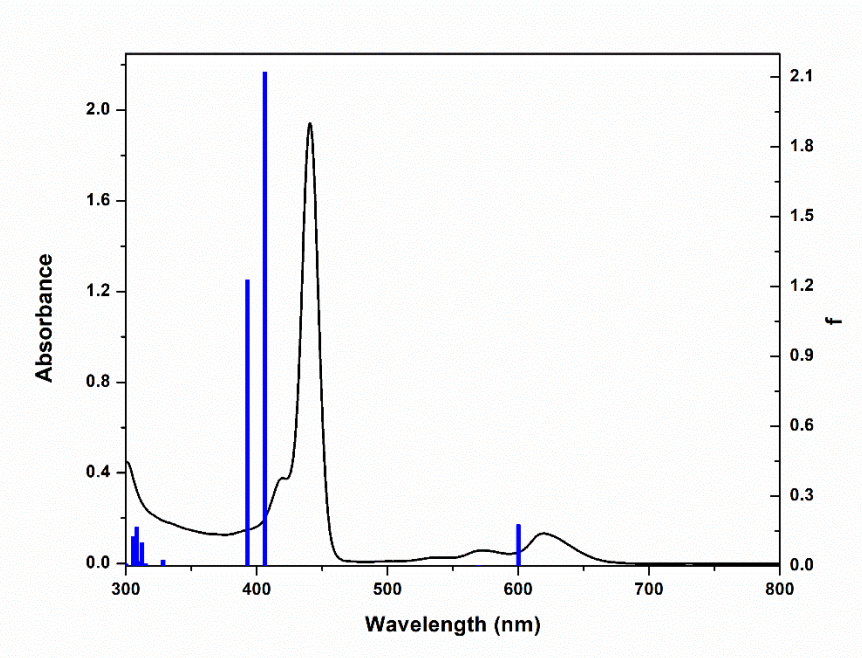

Figure S50. Calculated excitations (blue vertical lines) and experimental absorption spectra (black curve) for **2-Zn**.

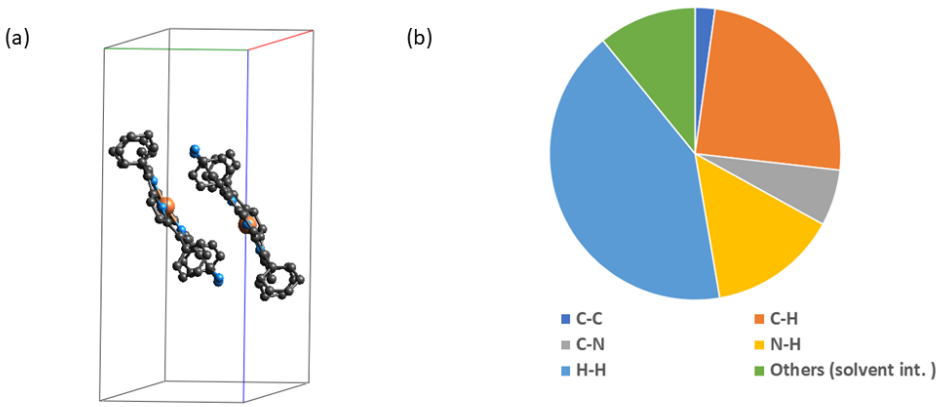

Figure S51. (a) Offset arrangement of molecules in crystal packing, and (b) Pie chart showing distribution of individual intermolecular interactions on the basis of Hirshfeld surface analysis.

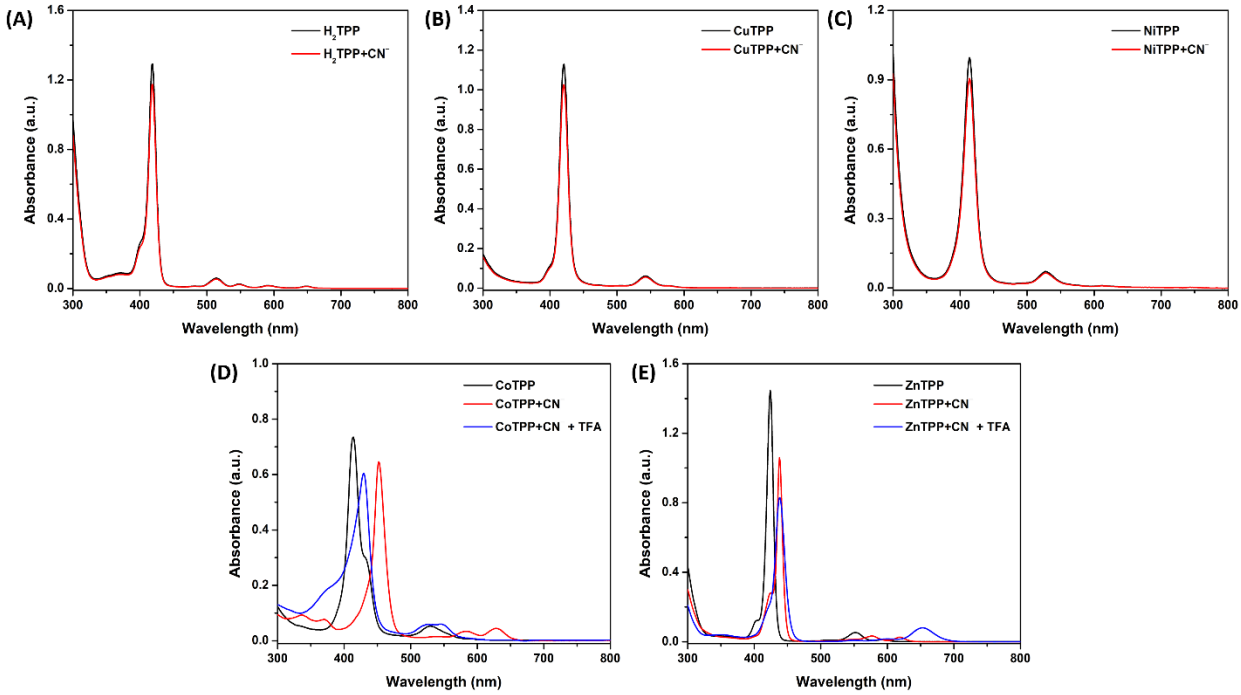

Figure S52. UV-vis spectra of parent porphyrins upon addition of excess cyanide in toluene at 298 K and reversibility study for CoTPP and ZnTPP under the influence of TFA.

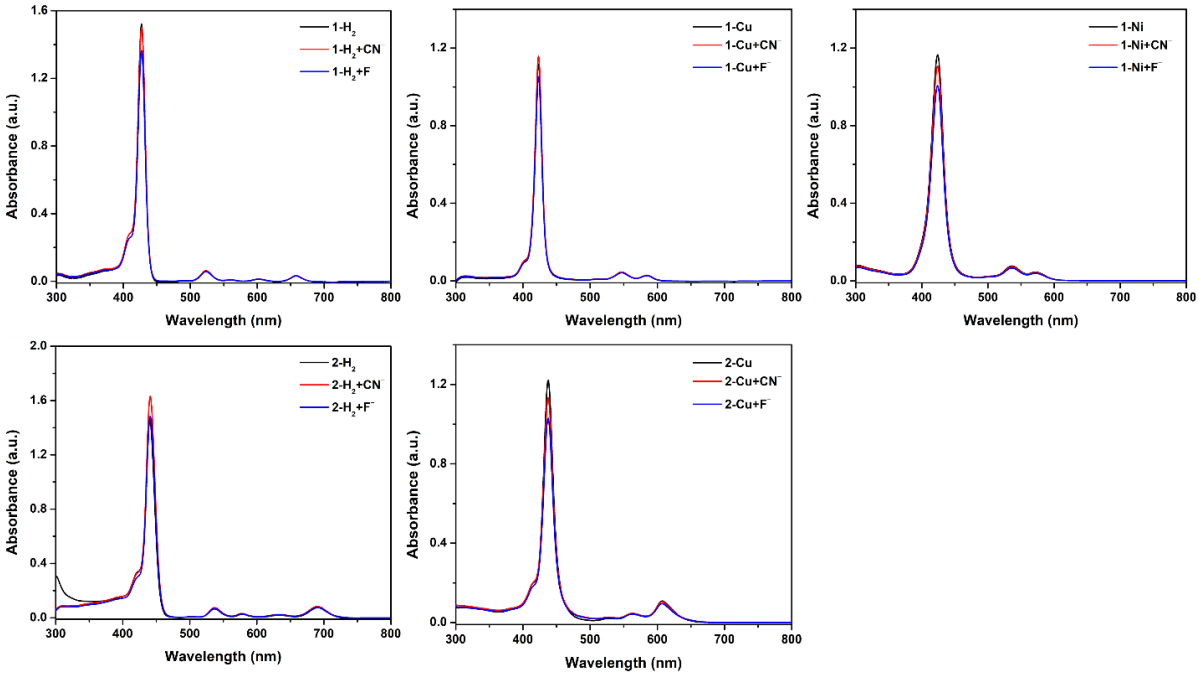

Figure S53. UV-vis spectra of porphyrins upon addition of excess cyanide and fluoride ions in toluene at 298 K.

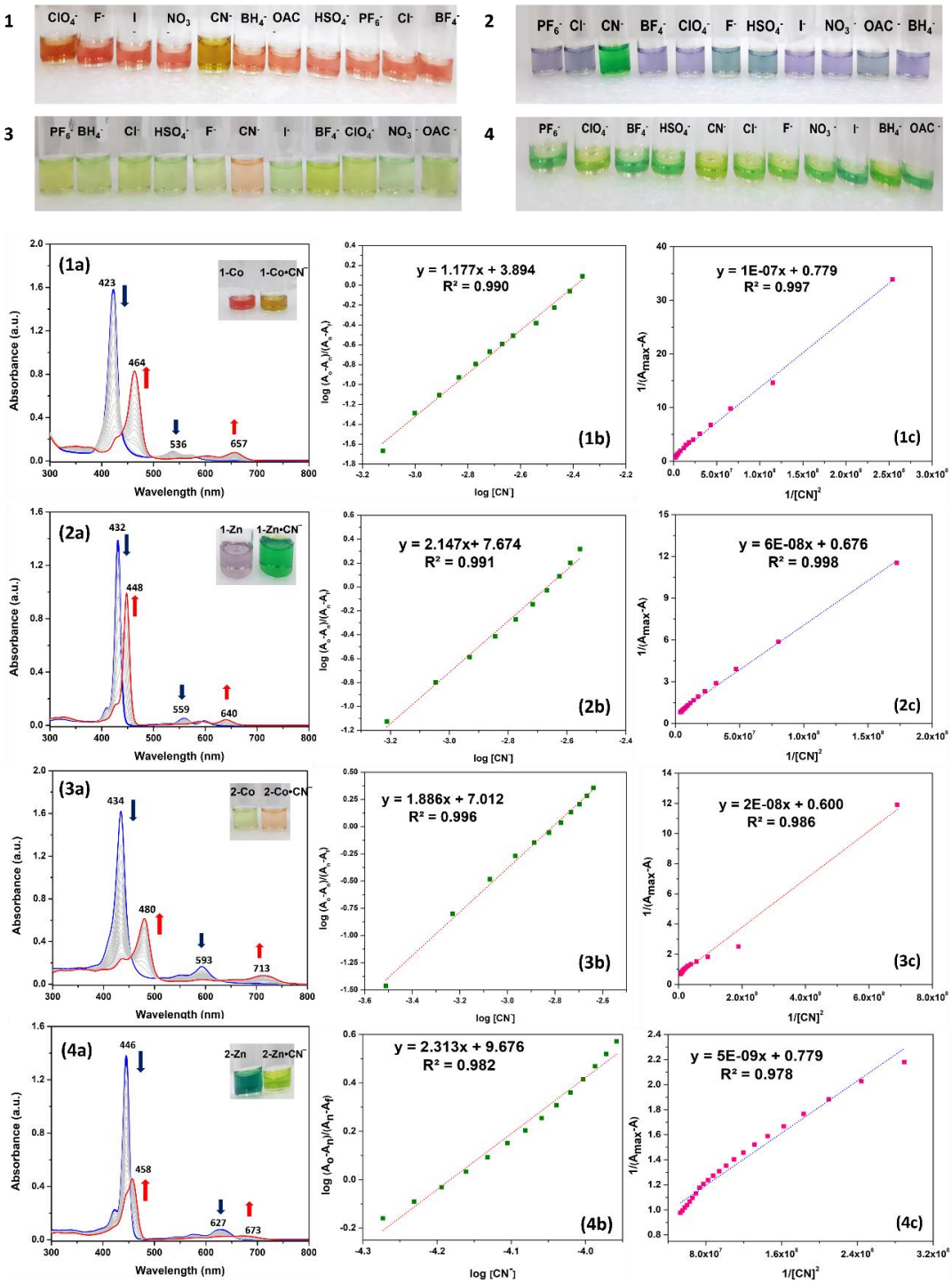

Figure S54. Color change of the electron-deficient porphyrins, 1-Co (1), 1-Zn (2), 2-Co (3) and 2-Zn (4) in the presence of different anionic solutions in the toluene at 298 K and UV-visible spectral titrations upon addition of aliquots of TBACN (0-1× 10^{-5} M) in toluene (a), corresponding Hill plot (b) and B-H plot (c).

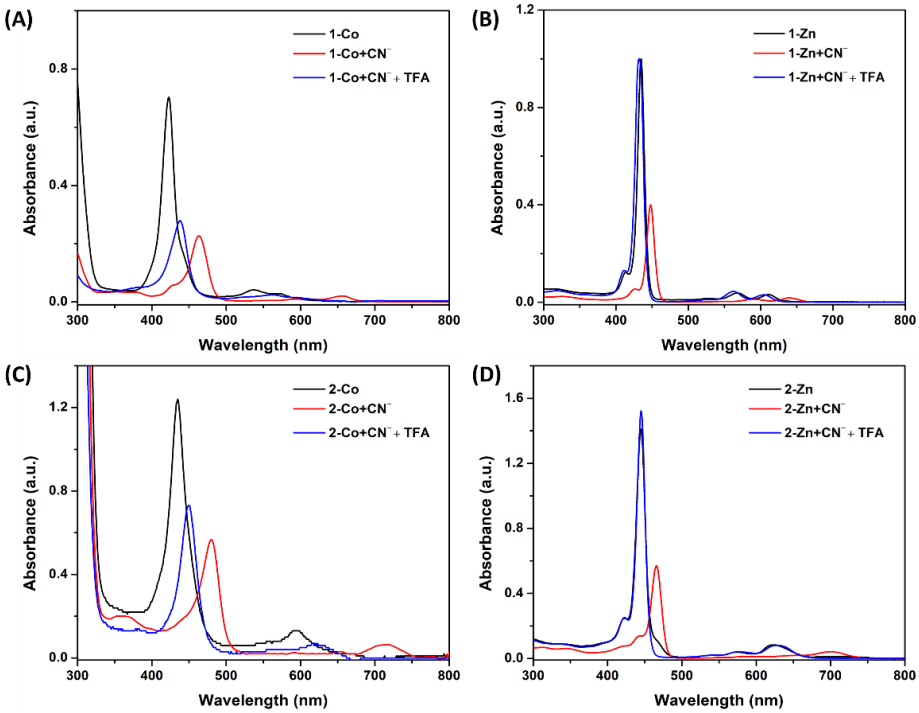

Figure S55. UV-visible spectra of **1-Co** (1), **1-Zn** (2), **2-Co** (3) and **2-Zn** (4) upon addition of cyanide ions and reversibility studies on addition of TFA.

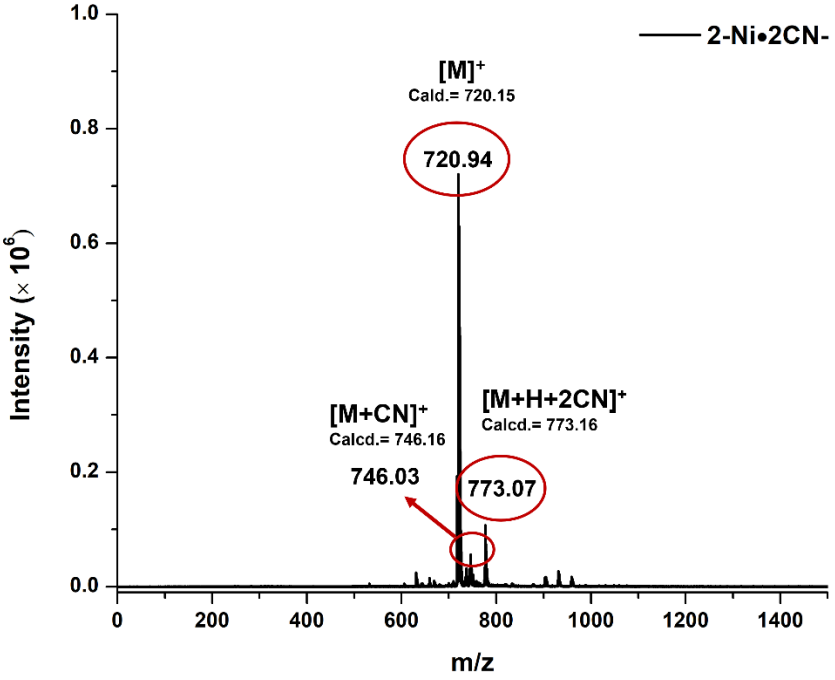

Figure S56. MALDI-TOF mass spectrum of 2-Ni in presence of cyanide ions.

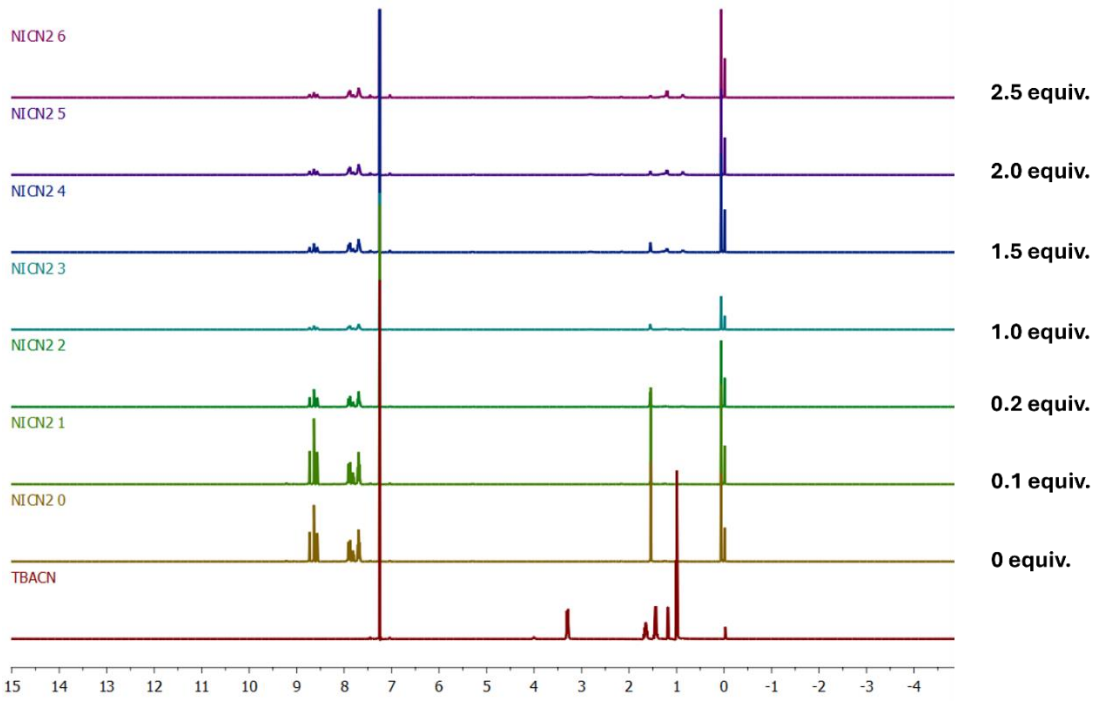

Figure S57. ^{1}H NMR titration of sensor **2-Ni** (5 mM) in $CDCl_3$ with adding 0 to 2.5 equivalence of TBACN.

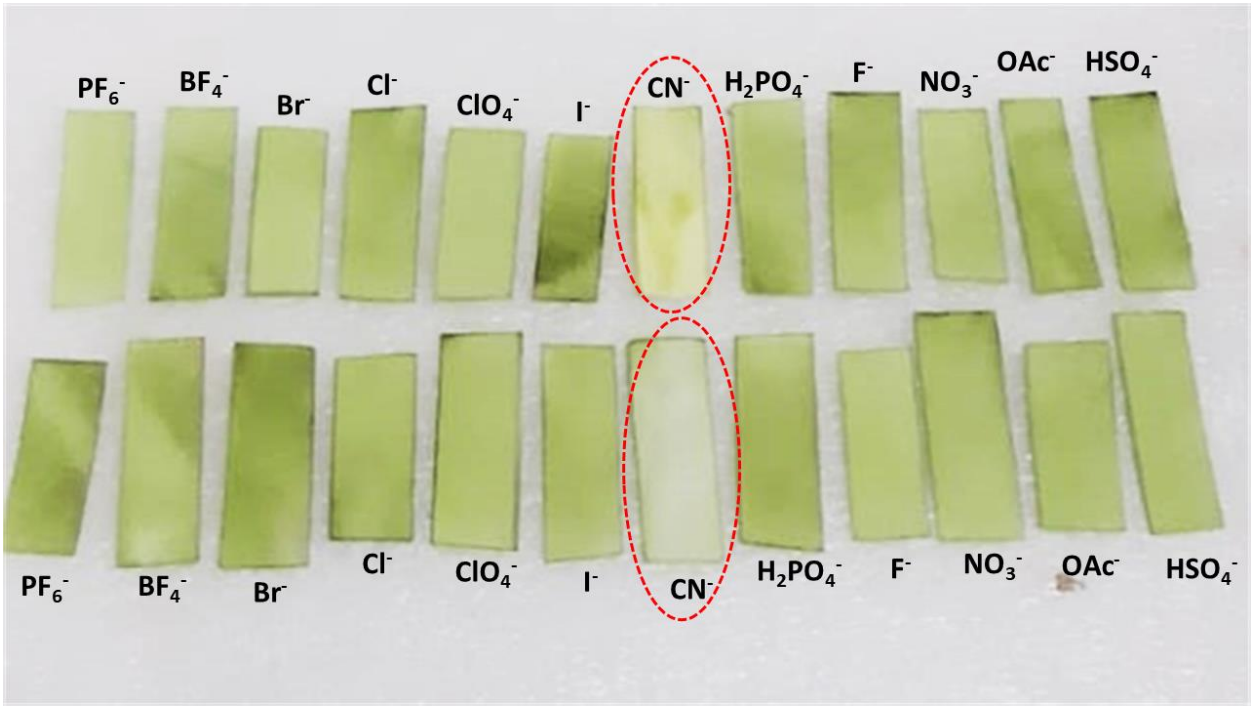

Figure S58. Photographs of test kits with **2-Ni** (1 mM) for detecting the cyanide ion in (a) toluene solution (above) and (b) neutral aqueous solution (below) with other anions.

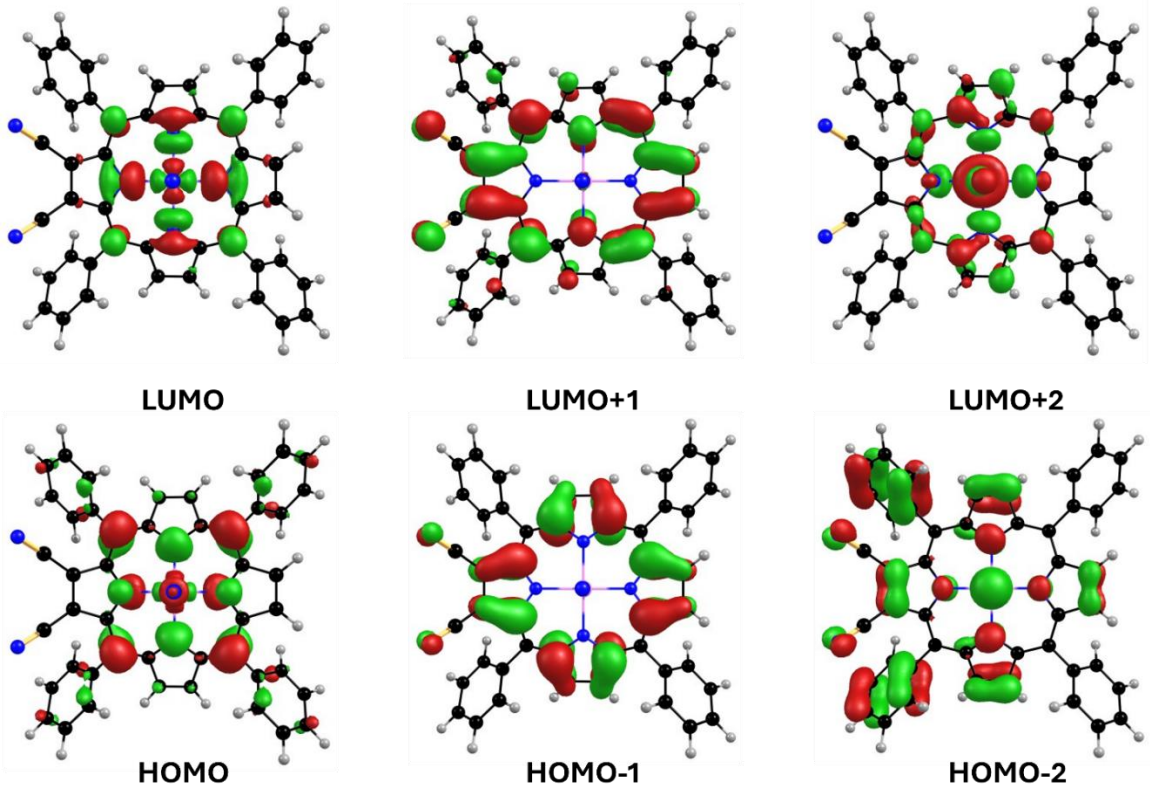

Figure S59. Frontier molecular orbitals of **2-Ni•2CN⁻**

Table S1. Data of selected bond angles (º) and bond lengths (Å) calculated from the single crystal XRD data analysis.

	$Cu(CN)_2$ **(2-Cu)**
Empirical Formula	C92H52Cu2N12
Formula Wt.	1571.90
Crystal System	Monoclinic
Space group	$P\text{-}2_1/n$
a (Å)	13.8547(7)
b (Å)	10.7681(6)
c (Å)	24.9017(14)
α (°)	90
β (°)	96.239(2)
γ (°)	90
Volume ($Å^3$)	3693.1(3)
Z	2
D_{calcd} (mg/m^3)	1.414
Wavelength (Å)	0.71073
T (°C)	296(2
No. of total reflns.	161008
No. of Independent reflns.	9550

R	0.0437
R_w	0.1167
GOOF	1.088
CCDC No.	2377991
Bond length (Å)	
M-N	1.999(17)
M-N’	1.975(17)
N-C$_\alpha$	1.378(3)
N’-C$_{\alpha'}$	1.378(3)
C$_\alpha$-C$_\beta$	1.436(3)
C$_{\alpha'}$-C$_{\beta'}$	1.441(3)
C$_\beta$-C$_\beta$	1.362(3)
C$_{\beta'}$-C$_{\beta'}$	1.339(3)
C$_\alpha$-C$_m$	1.396(3)
C$_{\alpha'}$-C$_m$	1.389(3)
ΔC$_\beta$ (Å)	0.439
Δ24 (Å)	0.247
ΔM	0.009
Bond Angles (°)	
M-N-C$_\alpha$	126.83(14)
M-N’-C$_{\alpha'}$	127.04(14)
N-M-N	173.47(7)
N’-M-N’	173.30(8)
N-C$_\alpha$-C$_m$	125.07(19)
N’-C$_{\alpha'}$-C$_m$	125.69(19)
N-C$_\alpha$-C$_\beta$	109.78(18)
N’-C$_{\alpha'}$-C$_{\beta'}$	109.68(19)
C$_\beta$-C$_\alpha$-C$_m$	124.89(19)
C$_{\beta'}$-C$_{\alpha'}$-C$_m$	124.37(19)
C$_\alpha$-C$_m$-C$_{\alpha'}$	123.52(19)
C$_\alpha$-C$_\beta$-C$_\beta$	107.05(19)
C$_{\alpha'}$-C$_{\beta'}$-C$_{\beta'}$	107.30(2)
C$_\alpha$-N-C$_\alpha$	106.23(17)
C$_{\alpha'}$-N-C$_{\alpha'}$	105.77(17)

Table S2. Data of selected bond angles (º) and bond lengths (Ǻ) calculated from ground state optimized geometries using B3LYP as functional and LANL2DZ as basis set.

	H_2TPP(CN) (**1-H_2**)	CoTPP(CN) (**1-Co**)	NiTPP(CN) (**1-Ni**)	CuTPP(CN) (**1-Cu**)	ZnTPP(CN) (**1-Zn**)
Bond length (Å)					
M - N	--	1.998	1.962	2.039	2.079
M - N′	--	1.988	1.953	2.024	2.063
N- C_α	1.382	1.401	1.398	1.397	1.395
N - $C_{\alpha'}$	1.385	1.400	1.398	1.397	1.396
C_α - C_β	1.463	1.451	1.450	1.453	1.457
$C_{\alpha'}$ - $C_{\beta'}$	1.439	1.452	1.452	1.455	1.458
C_β - C_β	1.363	1.375	1.376	1.377	1.380
$C_{\beta'}$ - $C_{\beta'}$	1.371	1.369	1.370	1.371	1.374
C_α - C_m	1.409	1.403	1.404	1.408	1.417
$C_{\alpha'}$ - C_m	1.403	1.401	1.402	1.406	1.415
Δ24	0.074	0.170	0.284	0.082	0.063
ΔC_β	0.166	0.309	0.282	0.195	0.141
ΔM	--	0.003	0.004	0.003	0.004
Bond Angle (°)					
N - M - N	--	177.81	178.44	179.77	178.83
N′ - M - N′	--	178.00	178.66	179.82	178.66
M - N - C_α	--	127.11	126.96	126.62	126.18
M - N′ - $C_{\alpha'}$	--	127.29	127.13	126.85	126.40
N - C_α - C_m	126.02	126.13	125.82	126.29	126.04
N′ - $C_{\alpha'}$ - C_m	126.99	126.32	125.98	126.59	126.33
N - C_α - C_β	110.00	110.04	109.89	109.48	108.94
N′ - $C_{\alpha'}$ - $C_{\beta'}$	106.35	110.24	110.09	109.68	109.13
C_β - C_α - C_m	123.97	123.80	124.04	124.23	125.01
$C_{\beta'}$- $C_{\alpha'}$ - C_m	126.66	123.40	123.67	123.73	124.53
C_α - C_m- $C_{\alpha'}$	125.24	122.08	120.89	123.23	125.06
C_α - N- C_α	106.27	105.55	105.84	106.54	107.40
$C_{\alpha'}$ - N- $C_{\alpha'}$	110.55	105.19	105.49	106.14	107.00

	H_2TPP$(CN)_2$ (**2-H_2**)	CoTPP$(CN)_2$ (**2-Co**)	NiTPP$(CN)_2$ (**2-Ni**)	CuTPP$(CN)_2$ (**2-Cu**)	ZnTPP$(CN)_2$ (**2-Zn**)
Bond length (Å)					
M - N	--	1.995	1.979	2.045	2.089
M - N′	--	1.981	1.962	2.016	2.055
N- C_α	1.380	1.400	1.399	1.396	1.395
N - $C_{\alpha'}$	1.387	1.400	1.400	1.397	1.396
C_α - C_β	1.465	1.451	1.450	1.454	1.458
$C_{\alpha'}$ - $C_{\beta'}$	1.441	1.454	1.453	1.456	1.459
C_β - C_β	1.374	1.382	1.382	1.384	1.387
$C_{\beta'}$ - $C_{\beta'}$	1.372	1.368	1.368	1.370	1.372

C_α - C_m	1.414	1.406	1.403	1.410	1.418
C_α' - C_m	1.405	1.401	1.399	1.406	1.414
Δ24	0.160	0.123	0.287	0.141	0.093
ΔC_β	0.337	0.490	0.552	0.282	0.203
ΔM	--	0.008	0.009	0.008	0.009
Bond Angle (°)					
N - M - N	--	175.76	174.45	178.71	179.49
N′ - M - N′	--	176.21	174.97	179.03	179.06
M - N - C_α	--	126.81	126.78	126.34	125.97
M - N′ - C_α'	--	127.12	127.09	126.71	126.36
N - C_α - C_m	125.86	125.75	125.54	126.00	125.86
N′ - C_α' - C_m	127.12	126.23	126.03	126.69	126.57
N - C_α - C_β	109.98	109.90	110.01	109.38	108.87
N′ - C_α' - C_β'	106.36	110.18	110.28	109.66	109.14
C_β - C_α - C_m	124.16	124.30	124.34	124.62	125.28
C_β'- C_α' - C_m	126.52	123.53	123.57	123.64	124.29
C_α - C_m- C_α'	124.85	121.85	121.04	123.05	124.68
C_α - N- C_α	106.67	105.85	105.65	106.85	107.71
C_α' - N- C_α'	110.58	105.24	105.06	106.15	106.97

Table S3. TD-DFT calculated one-electron transitions and oscillator strengths of monocyano porphyrin and dicyano porphyrins. (f > 0.01).

Porphyrin	**Excited state**	**λ_{max}**	**f**	**Orbital composition**	**Energy (eV)**	**Major contribution (%)**
1-H_2	1	605.76	0.0948	HOMO→LUMO	2.0468	60
	3	386.18	1.8616	HOMO-1→LUMO	3.2105	45
	4	380.54	1.7398	HOMO-1→LUMO+1	3.2581	52
	6	309.89	0.5022	HOMO-3→LUMO	4.0010	58
1-Co	11	561.70	0.0634	HOMO→LUMO	2.2073	68
	18	395.93	1.4247	HOMO-1→LUMO+1	3.1314	43
				HOMO→LUMO		22
	20	392.49	1.5983	HOMO-1→LUMO	3.1589	34
1-Ni	4	546.91	0.0775	HOMO→LUMO	2.2670	57
	7	393.21	1.7877	HOMO→LUMO+1	3.1532	49
				HOMO-1→LUMO		50
	8	387.86	1.4494	HOMO-1→LUMO+1	3.1966	58
1-Cu	6	555.45	0.0841	HOMO→LUMO	2.2321	63
	14	395.52	1.7798	HOMO-1→LUMO	3.1347	50
	15	389.66	1.3402	HOMO-1→LUMO+1	3.1819	55
1-Zn	1	574.58	0.1099	HOMO→LUMO	2.1578	60
	3	396.59	1.9893	HOMO-1→LUMO	3.1262	53
	4	388.81	1.6397	HOMO-1→LUMO+1	3.1888	60

Porphyrin	Excited state	λ_{max}	f	Orbital composition	Energy (eV)	Major contribution (%)
2-H_2	1	636.37	0.1039	HOMO→LUMO	1.9483	62
	3	401.65	2.0966	HOMO-1→LUMO	3.0869	46
	4	396.80	1.2564	HOMO-1→LUMO+1	3.1246	59
2-Co	10	592.30	0.1588	HOMO→LUMO	2.0933	57
	12	550.33	0.0137	HOMO-1→LUMO	2.2529	64
	18	401.23	1.7025	HOMO→LUMO+1	3.0901	50
	20	395.53	0.6041	HOMO-1→LUMO+1	3.1346	56
2-Ni	4	567.28	0.1553	HOMO→LUMO	2.1856	62
	7	401.96	1.8841	HOMO→LUMO+1	3.0845	51
	8	392.19	1.1170	HOMO-1→LUMO+1	3.1613	62
2-Cu	5	596.13	0.1701	HOMO→LUMO	2.0798	64
	15	431.67	1.5343	HOMO-1→LUMO	2.8722	49
	18	421.11	0.6191	HOMO-1→LUMO+1	2.9442	56
	21	396.34	0.0112	HOMO-2→LUMO	3.1282	49
2-Zn	1	599.90	0.1763	HOMO→LUMO	2.0668	63
	3	406.18	2.1207	HOMO-1→LUMO	3.0524	52
				HOMO→LUMO+1		48
	4	392.78	1.2262	HOMO-1→LUMO+1	3.1566	63